Progress In Electromagnetics Research B, Vol. 72, 129–148, 2017

Reconstruction of the *S*-Matrix of *N*-Port Waveguide Reciprocal Devices from 2-Port VNA Measurements

Leonardo Zappelli*

Abstract—Two approaches to reconstruct the S-matrix of N-port waveguide reciprocal devices from 2-port S-matrix measurements are proposed and discussed. The main advantage of the proposed approaches is that measurements are done always at the same two ports, without moving the device. The remaining N-2 ports are loaded with different loads, either matched or short. The first approach, based on a manipulation of the 2-port S-matrices, requires N-2 matched and two other loads, while the second approach, based on the evaluation of an equivalent circuit, requires N-2 short and two other loads. The measurement technique is based on standard loads (short, shift and matched) in the waveguide calibration kit of the 2-port VNA.

1. INTRODUCTION

2-port vector network analyzer (VNA) is a common measurement equipment used in microwave laboratories. Its development is principally due to the contribution of Speciale and his research group [1]. During the years, alternative calibrations or some refinement procedures to enhance the calibration of 2-port VNA were proposed by several authors [2–5].

Recently, multi-port devices have been proposed for many applications, and they need very expensive N-port VNA to perform the requested measurements. Hence, some techniques to perform measurements of N-port devices with 2-port VNA were analyzed and discussed [6–18].

The most used method to perform N-port measurements with 2-port VNA consists in the excitation of 2 ports, i and j, loading the remaining N-2 ports with proper loads. This implies several disconnections of the device under test (DUT) [7, 9, 12] or the implementation (and realization) of switch-matrices to excite ports i and j to perform measurements [8, 10, 14–17]. Moreover, the possibility of reducing the number of known loads [14, 15] or the use of virtual loads [18] have been analyzed.

Another technique consists in fixing two measurement ports, loading the other N-2 ports with proper loads, without disconnecting the DUT several times [11, 13]. In [11], the measurement of 3-port devices is discussed: 2 ports are connected to the VNA, and the third is loaded with three different loads to obtain the overall 3-port S-matrix. This approach is useful for a 3-port device but questionable for devices with more ports [19]. In [13], the approach used in [11] is partially used, and two port-reduction methods are proposed to reconstruct N-port S-matrix with a reduction of the connections to the VNA.

The aim of this paper is to refine these techniques to reconstruct N-port S-matrix of waveguide reciprocal devices using 2-port VNA, performing measurements always at the same two ports, without moving the DUT, and taking into account the presence of the VNA calibration kit. In particular, the FLANN calibration kit for WR90 waveguide contains: two shorts, two matched loads and two waveguides of lengths $\frac{\lambda}{8}$ and $\frac{3\lambda}{8}$, hereinafter called "$\frac{\lambda}{8}$ shift" and "$\frac{3\lambda}{8}$ shift". This equipment is sufficient to measure up to 4-port waveguide devices, while for 5 or more ports other components are needed.

Received 24 October 2016, Accepted 5 January 2017, Scheduled 24 January 2017

* Corresponding author: Leonardo Zappelli (l.zappelli@univpm.it).
The author is with the Dipartimento di Ingegneria dell'Informazione, Università Politecnica delle Marche, Via Brecce Bianche, Ancona 60131, Italy.

The approaches proposed in this paper are two. The first is a deep variation of the approach used in [11], which will be defined as "S-direct" approach. The second is a new approach based on the reconstruction of an equivalent circuit for N-port waveguide device, based on 2-port VNA measurements, which will be defined as "EC" (Equivalent Circuit) approach. This approach starts from the possibility of defining a set of equivalent circuits for a device, in the sense defined by Marcuvitz [20] and Montgomery [21]: an equivalent circuit can represent a simple frequency dependence or the minimization of the electrical parameters, or the effects of evanescent modes.... Hence, any device can be represented with various equivalent circuits, and each one represents a particular characteristic and is "correct".

In the past, the author has defined some equivalent circuits to represent the presence of evanescent accessible modes and a fast and simple method for the identification of the electrical parameters of the equivalent circuits for waveguide devices [22–25]. Hence, in the second approach an equivalent circuit will be proposed to reconstruct the N-port S-matrix waveguide device, starting from 2-port VNA measurements, in order to minimize and simplify the evaluation of its $N(N+1)/2$ circuit parameters. Afterwards, the N-port Z-matrix can be obtained by applying the Kirchhoff's Voltage Law (KVL) to the circuit, and the S-matrix is evaluated by the usual matrix manipulations.

The results show good agreement for the two approaches. Only the scattering parameters with very low value ($< -35\,\mathrm{dB}$) could contain errors in their evaluation, related to the quality of the loads and to VNA measurement uncertainty.

2. THEORY

2.1. *S*-Direct Approach

The first method to reconstruct the S-matrix of a reciprocal waveguide device based on 2-port VNA measurements is based on the approach discussed in [11]. In this paper, Davidovitz proposed a method to reconstruct the S-matrix of a 3-port device, based on three sets of 2-port VNA measurements. In particular, the third port of the device is closed on three different loads. In absence of experimental errors, the reconstruction is correct. Though the approach is valid, the extension to the measurement of S-matrix of devices with more ports is not trivial [19]. Moreover, the presence of experimental errors can cause an incorrect reconstruction. The important reading key of [11] is that all the measurements are done always at the same two ports, without disconnecting and reconnecting the device, as instead is done in most papers cited in the Introduction. To avoid the disconnection and reconnection, switching matrices must be developed and inserted between the VNA ports and the device, increasing the cost of the overall equipment. To the Author's opinion, the approach used in [11] is very interesting because the disconnection and reconnection of the device can cause supplementary measurement errors. In fact, it is well known that if we measure the S-matrix of a 2-port device and we disconnect and reconnect the second port of the same device to the VNA, the measured S-matrix in the second case has different values for the transmission and for the reflection at the second port. Obviously, the differences are small and explainable, firstly, in terms of correct alignment of the device in the second reconnection (which can be reduced with the presence of precision dowels at the flanges of the device and of the waveguide-coax adaptors) and, secondly, to the unwanted movements of the cable connecting the second port of the device and the VNA, during the phase of device re-connection.

On the contrary, the main advantage in blocking the two ports used to measure the N-port device is that the cable disposition to connect the device and the VNA is fixed, and no other measurements errors due to the cable movements are introduced. Moreover, the cost of the measurement procedure proposed in [11] is limited to the cost of the calibrated loads, because switching matrices are not used. Hence, in order to reduce these measurement errors and cost of the overall measurements, the technique of fixing the two measurement ports (ports 1 and 2) should be used, and the reconstruction of the N-port S-matrix should be based on loading the remaining N-2 ports with three different loads connected to each port in a proper way that will be discussed in the following. How can we choose these loads? The simplest choice is to use just the standard loads contained in the VNA calibration kit, as stated in the Introduction: two shorts, two matched loads and a $\frac{\lambda}{8}$ shift and a $\frac{3\lambda}{8}$ shift. The main advantage is that they are well realized and certified; for example, the $\frac{\lambda}{8}$ shift and $\frac{3\lambda}{8}$ shift contained in our FLANN

kit for WR-90 waveguides are certified to have lengths $t_a = 4.835\,\text{mm}$ and $t_b = 14.458\,\text{mm}$, respectively.

For a 3-port device, the procedure to evaluate its 3-port S-matrix consists in loading port 3 with a matched load and two different loads and measuring the three corresponding 2-port reduced devices with the VNA always connected to ports 1 and 2. The two loads can be chosen between the three combinations, shown in Table 1, that can be obtained with the calibration kit. "$\frac{\lambda}{8}$ & short" and "$\frac{3\lambda}{8}$ & short" stand for $\frac{\lambda}{8}$ shift (length t_a) and $\frac{3\lambda}{8}$ shift (length t_b) connected to a short. The obtained three 2-port S-matrices, S^{I}, S^{II} and S^{III}, permit the reconstruction of the 3-port S-matrix [11]. The superscripts I, II and III refer to three loads connected to port 3, chosen in Table 1. The first measurement, S^{I}, done with the matched load connected to port 3, gives the scattering coefficients S_{11}, S_{12} and S_{22}.

Table 1. Possible combination of loads connected to port 3. "$\frac{\lambda}{8}$ & short" and "$\frac{3\lambda}{8}$ & short" stand for $\frac{\lambda}{8}$ shift (length t_a) or $\frac{3\lambda}{8}$ shift (length t_b) connected to a short. Γ is the load reflection coefficient.

	Load I	Γ_{I}	Load II	Γ_{II}	Load III	Γ_{III}
(a)	matched	0	short	-1	$\frac{\lambda}{8}$ & short	$-\text{e}^{-2\text{j}\beta t_a}$
(b)	matched	0	short	-1	$\frac{3\lambda}{8}$ & short	$-\text{e}^{-2\text{j}\beta t_b}$
(c)	matched	0	$\frac{\lambda}{8}$ & short	$-\text{e}^{-2\text{j}\beta t_a}$	$\frac{3\lambda}{8}$ & short	$-\text{e}^{-2\text{j}\beta t_b}$

Unfortunately, [11] does not analyze the redundancy of the obtained measurements. In fact, in the hypothesis of a reciprocal device, S^{II} (three complex numbers, $S^{\text{II}}_{11}, S^{\text{II}}_{12}, S^{\text{II}}_{22}$) and S^{III} (three complex numbers, $S^{\text{III}}_{11}, S^{\text{III}}_{12}, S^{\text{III}}_{22}$) are composed of six complex scattering parameters, while the scattering parameters of the 3-port S-matrix to be evaluated are only three, because S_{11}, S_{12} and S_{22} have already been measured. Hence, three measured scattering parameters are redundant, and they are linearly dependent on the other three. The relationships between the three unknown independent parameters and the three linear dependent scattering parameters can be easily found. In fact, if we start from the measurement of S^I and assume its scattering parameters as linearly independent, only two scattering parameters of S^{II} and only one scattering parameter of S^{III} are linearly independent.

This can be shown starting from the evaluation of the reduced 2-port S-matrix ($S^{3\to 2}$), obtained by connecting the third port of the 3-port S-matrix to a load with reflection coefficient Γ,

$$S^{3\to 2} = \begin{bmatrix} S_{11} + \dfrac{S_{13}^2\Gamma}{1 - S_{33}\Gamma} & S_{12} + \dfrac{S_{13}S_{23}\Gamma}{1 - S_{33}\Gamma} \\ S_{12} + \dfrac{S_{13}S_{23}\Gamma}{1 - S_{33}\Gamma} & S_{22} + \dfrac{S_{23}^2\Gamma}{1 - S_{33}\Gamma} \end{bmatrix} \tag{1}$$

With simple mathematical steps, we can write the three redundant scattering parameters of the three measured 2-port S-matrices, obtained with three different loads connected to port 3, characterized by reflection coefficients $\Gamma_{\text{I}} = 0, \Gamma_{\text{II}}, \Gamma_{\text{III}}$, in the following form:

$$S^{\text{II}}_{22} = S^{\text{I}}_{22} - \frac{\left(S^{\text{I}}_{12} - S^{\text{II}}_{12}\right)^2}{S^{\text{I}}_{11} - S^{\text{II}}_{11}} \qquad S^{\text{III}}_{12} = \frac{-S^{\text{II}}_{11}S^{\text{I}}_{12} + S^{\text{III}}_{11}\left(S^{\text{I}}_{12} - S^{\text{II}}_{12}\right) + S^{\text{I}}_{11}S^{\text{II}}_{12}}{S^{\text{I}}_{11} - S^{\text{II}}_{11}} \tag{2}$$

$$S^{\text{III}}_{22} = S^{\text{I}}_{22} - \frac{\left(S^{\text{I}}_{11} - S^{\text{III}}_{11}\right)\left(S^{\text{I}}_{12} - S^{\text{II}}_{12}\right)^2}{\left(S^{\text{I}}_{11} - S^{\text{II}}_{11}\right)^2} \tag{3}$$

In Eqs. (2)–(3), the independence of $S^{\text{I}}_{11}, S^{\text{I}}_{12}, S^{\text{I}}_{22}, S^{\text{II}}_{11}, S^{\text{II}}_{12}, S^{\text{III}}_{11}$ has been supposed. With this choice, the values of the scattering parameters of the reconstructed 3-port S-matrix are:

$$S_{23} = \pm\left(S^{\text{I}}_{12} - S^{\text{II}}_{12}\right)\sqrt{\frac{\left(\Gamma_{\text{II}} - \Gamma_{\text{III}}\right)\left(S^{\text{I}}_{11} - S^{\text{III}}_{11}\right)}{\Gamma_{\text{II}}\Gamma_{\text{III}}\left(S^{\text{I}}_{11} - S^{\text{II}}_{11}\right)\left(S^{\text{II}}_{11} - S^{\text{III}}_{11}\right)}} \tag{4}$$

$$S_{13} = \frac{(S_{11}^{\mathrm{I}} - S_{11}^{\mathrm{II}})S_{23}}{S_{12}^{\mathrm{I}} - S_{12}^{\mathrm{II}}} \qquad S_{33} = \frac{S_{11}^{\mathrm{I}} - S_{11}^{\mathrm{II}}}{\left(S_{12}^{\mathrm{I}} - S_{12}^{\mathrm{II}}\right)^2} S_{23}^2 + \frac{1}{\Gamma_{\mathrm{II}}} \tag{5}$$

$$S_{11} = S_{11}^{\mathrm{I}} \qquad S_{12} = S_{12}^{\mathrm{I}} \qquad S_{22} = S_{22}^{\mathrm{I}} \tag{6}$$

Obviously, any other choice of the three linearly independent scattering parameters is correct, producing different relationships of the linearly dependent scattering parameters, similar to Eqs. (2)–(3), and different expressions for the scattering parameters, similar to Eqs. (4)–(5). The possible choices of the three independent parameters are nine and are shown in Table 2. In absence of experimental errors, Equations (2)–(3) are always satisfied, and any choice of the three independent scattering parameters gives always the same 3-port S-matrix. In presence of experimental errors, the scenario is slightly different with respect to the approach discussed in [11]. In fact, the linear dependent scattering parameters do not satisfy Eqs. (2)–(3) just for the experimental errors occurring on all measured scattering parameters. Moreover, the user does not know which are the "most correct" three independent parameters, and this fact produces an uncertainty in the S-matrix reconstruction. Hence, the user must take into account all the nine combinations of the independent parameters, obtaining nine possible 3-port S-matrices.

Table 2. Possible combinations of the linearly independent scattering parameters. S^{II} and S^{III} are 2-port S-matrices measured with the third port of the device connected to two different loads.

1	S_{11}^{II}	S_{12}^{II}	S_{11}^{III}		2	S_{11}^{II}	S_{12}^{II}	S_{12}^{III}		3	S_{11}^{II}	S_{12}^{II}	S_{22}^{III}
4	S_{11}^{II}	S_{22}^{II}	S_{11}^{III}		5	S_{11}^{II}	S_{22}^{II}	S_{12}^{III}		6	S_{11}^{II}	S_{22}^{II}	S_{22}^{III}
7	S_{12}^{II}	S_{22}^{II}	S_{11}^{III}		8	S_{12}^{II}	S_{22}^{II}	S_{12}^{III}		9	S_{12}^{II}	S_{22}^{II}	S_{22}^{III}

Moreover, to take into account all the possible combinations, the user must consider as second load any of the chosen loads, in order to ensure that three independent parameters belong to S^{II} or to S^{III}. For example, for the first row of Table 1, the user should evaluate the reconstructed 3-port S-matrix for the following two combinations of the same three loads:

(i) matched, short, $\frac{\lambda}{8}$ & short,

(ii) matched, $\frac{\lambda}{8}$ & short, short.

In so doing, the user changes the first two independent scattering parameters, associating them to the 2-port S-matrix measured with a short (item i) or a $\frac{\lambda}{8}$ & short (item ii) connected to port 3. Hence, the total possible combinations of the reconstructed 3-port S-matrix corresponding to each row of Table 1 are 18 : 9 (the combinations of the chosen independent scattering parameters shown in Table 2) $\times 2$ (possible choices of the order of the second and third loads). The average of the 18 values of each scattering parameter is applied to find the most correct 3-port S-matrix. Averaging improves the evaluation of the scattering parameters if the experimental errors are not systematic.

In presence of a reciprocal device with four ports, the previous approach becomes more complex. In fact, if two loads with reflection coefficients γ_3, γ_4 are connected to ports 3 and 4 of a 4-port S-matrix, the following 2-port S-matrix is obtained:

$$\begin{aligned} S_{11}^{4\to 2} = {} & \left\{2S_{13}S_{14}S_{34}\gamma_3\gamma_4 + S_{14}^2(1 - S_{33}\gamma_3)\gamma_4 + S_{13}^2(1 - S_{44}\gamma_4)\gamma_3 + S_{11}\left[1 - S_{44}\gamma_4 - S_{33}\gamma_3\right.\right. \\ & \left.\left. + \gamma_3\gamma_4(S_{33}S_{44} - S_{34}^2)\right]\right\} / \left[1 - S_{44}\gamma_4 - S_{33}\gamma_3 + \left(S_{33}S_{44} - S_{34}^2\right)\gamma_3\gamma_4\right] \end{aligned} \tag{7}$$

$$\begin{aligned} S_{12}^{4\to 2} = {} & \left\{S_{14}(S_{24} - S_{24}S_{33}\gamma_3 + S_{23}S_{34}\gamma_3)\gamma_4 + S_{13}(S_{23} + S_{24}S_{34}\gamma_4 - S_{23}S_{44}\gamma_4)\gamma_3 + S_{12}\left(1 - S_{44}\gamma_4\right)\right. \\ & \left. + S_{12}\left[\gamma_3\gamma_4(S_{33}S_{44} - S_{34}^2) - S_{33}\gamma_3\right]\right\} / \left[1 - S_{44}\gamma_4 - S_{33}\gamma_3 + \left(S_{33}S_{44} - S_{34}^2\right)\gamma_3\gamma_4\right] \end{aligned} \tag{8}$$

$$\begin{aligned} S_{22}^{4\to 2} = {} & \left\{2S_{23}S_{24}S_{34}\gamma_3\gamma_4 + S_{24}^2(1 - S_{33}\gamma_3)\gamma_4 + S_{23}^2(\gamma_3 - S_{44}\gamma_3\gamma_4) + S_{22}\left[1 - S_{44}\gamma_4 - S_{33}\gamma_3\right.\right. \\ & \left.\left. + \gamma_3\gamma_4(S_{33}S_{44} - S_{34}^2)\right]\right\} / \left[1 - S_{44}\gamma_4 - S_{33}\gamma_3 + \left(S_{33}S_{44} - S_{34}^2\right)\gamma_3\gamma_4\right] \end{aligned} \tag{9}$$

The procedure to reconstruct the 4-port S-matrix consists in loading port 3 with three loads, being a load connected to port 4, then loading port 4 with three loads, being one of the previous load

connected to port 3, and, finally, loading ports 3 and 4 with two loads in a combination not used in the previous cases. Six 2-port S-matrices are measured (18 complex scattering parameters are measured) to find 10 complex scattering parameters of the 4-port S-matrix: even in this case, there is measurement redundancy. Unfortunately, an approach similar to that discussed for a 3-port device, i.e., to find some equations as Eqs. (2)–(3) and Eqs. (4)–(6), is quite difficult to apply because it is not easy to solve Eqs. (7)–(9) for the scattering parameters of the four-port S-matrix. Nevertheless, the solution to this problem exists, if two calibrated matched loads are available, as in the calibration kit.

In fact, if the first matched load is connected to port 4 ($\gamma_4 = 0$), the 4-port S-matrix reduces to a 3-port S-matrix containing only the scattering parameters of the first 3 ports ($S_{11}, S_{12}, S_{13}, S_{22}, S_{23}, S_{33}$), which can be reconstructed connecting three loads to port 3, with a combination chosen between the first three rows (a)–(c) of Table 1, including the second matched load. The procedure to reconstruct these six scattering parameters follows the previously discussed approach in Eqs. (4)–(6).

Afterwards, the first matched load is connected to port 3, and in this case, the 4-port S-matrix reduces to a 3-port S-matrix containing only the scattering parameters relative to ports 1, 2 and 4 ($S_{11}, S_{12}, S_{14}, S_{22}, S_{24}, S_{44}$), which can be reconstructed with Eqs. (4)–(6), connecting port 4 to three loads, chosen in rows (a)–(c) of Table 1, including the second matched load. It should be noted that only two measurements must be made, because the combination of the two matched loads at ports 3 and 4 has already been measured when the first six scattering parameters relative to port 3 are reconstructed.

The last scattering parameters S_{34} is obtained loading ports 3 and 4 with a combination of two loads, characterized by reflection coefficients γ_3, γ_4, without the use of matched loads. The seven possible combinations are shown in Table 3, cases (a)–(g), with $i = 3$ and $j = 4$.

Table 3. Possible combinations of loads, with reflection coefficient γ, to be connected to ports i and j.

	Port i load	γ_i	Port j load	γ_j		Port i load	γ_i	Port j load	γ_j
(a)	short	-1	short	-1	(b)	short	-1	$\frac{\lambda}{8}$ & short	$-\mathrm{e}^{-2\mathrm{j}\beta t_a}$
(c)	short	-1	$\frac{3\lambda}{8}$ & short	$-\mathrm{e}^{-2\mathrm{j}\beta t_a}$	(d)	$\frac{\lambda}{8}$ & short	$-\mathrm{e}^{-2\mathrm{j}\beta t_a}$	short	-1
(e)	$\frac{3\lambda}{8}$ & short	$-\mathrm{e}^{-2\mathrm{j}\beta t_b}$	short	-1	(f)	$\frac{\lambda}{8}$ & short	$-\mathrm{e}^{-2\mathrm{j}\beta t_a}$	$\frac{3\lambda}{8}$ & short	$-\mathrm{e}^{-2\mathrm{j}\beta t_b}$
(g)	$\frac{3\lambda}{8}$ & short	$-\mathrm{e}^{-2\mathrm{j}\beta t_b}$	$\frac{\lambda}{8}$ & short	$-\mathrm{e}^{-2\mathrm{j}\beta t_a}$	(h)	$\frac{\lambda}{8}$ & short	$-\mathrm{e}^{-2\mathrm{j}\beta t_a}$	matched load	0
(i)	$\frac{3\lambda}{8}$ & short	$-\mathrm{e}^{-2\mathrm{j}\beta t_b}$	matched load	0	(j)	matched load	0	matched load	0

The last measurement gives a scattering matrix $S^{\gamma_3\gamma_4}$ (three scattering parameters $S_{11}^{\gamma_3\gamma_4}, S_{12}^{\gamma_3\gamma_4}, S_{22}^{\gamma_3\gamma_4}$) that permits to obtain S_{34} from one of Eqs. (7)–(9), for example from Eq. (7):

$$S_{34} = \frac{S_{13}S_{14}}{S_{11} - S_{11}^{\gamma_3\gamma_4}} \pm \frac{\sqrt{S_{13}^2\gamma_3 + (S_{11} - S_{11}^{\gamma_3\gamma_4})(1 - S_{33}\gamma_3)}}{(S_{11} - S_{11}^{\gamma_3\gamma_4})\sqrt{\gamma_3\gamma_4}} \sqrt{S_{14}^2\gamma_4 + (S_{11} - S_{11}^{\gamma_3\gamma_4})(1 - S_{44}\gamma_4)} \quad (10)$$

The uncertainty about the sign of the square root is solved by replacing both values of S_{34} in Eq. (7) and verifying which sign of the square root in Eq. (10) gives the correct values of $S_{11}^{\gamma_3\gamma_4}, S_{12}^{\gamma_3\gamma_4}, S_{22}^{\gamma_3\gamma_4}$.

In absence of experimental errors, any choice of Eqs. (7)–(9) gives always the same S_{34}. In presence of experimental errors, the values of S_{34} that solve each of Eqs. (7)–(9) must be obtained, for a total of three possible values. The average of these values is applied to find the most correct value for S_{34}.

The same approach can be used to reconstruct the S-matrix of N-port devices with measurements performed always at ports 1 and 2. In this case, N-2 matched loads are needed, and the measurement procedure is the application of the procedure for a 4-port device at different port combinations:

(i) load ports 3, 4, ..., N with N-2 matched loads and measure the S-matrix to obtain S_{11}, S_{12}, S_{22}.

(ii) load ports 4, 5, ..., N with N-3 matched loads, and port 3 with two different loads, chosen between the combinations (a)–(c) of Table 1, and measure the two 2-port S-matrices at port 1 and 2, to obtain the scattering parameters S_{13}, S_{23}, S_{33} with (4)–(6).

(iii) repeat step 2) for port 4, to obtain S_{14}, S_{24}, S_{44}.

(iv) ...

(v) repeat step 2) for port N, to obtain S_{1n}, S_{2n}, S_{nn}.

(vi) load ports 3 and 4 with one combination of loads chosen between cases (a)–(g) of Table 3, and ports 5, ..., N with N-2 matched loads, and measure the S-matrix at port 1 and 2, to obtain the scattering parameters S_{34} with (10).

(vii) repeat step 7) for ports 3 and 5, to obtain S_{35}.

(viii) repeat step 7) for ports i and j ($3 \le i \le N-1, i+1 \le j \le N$), to obtain S_{ij}.

2.2. Equivalent Circuit Approach (*EC*-Approach)

The second proposed approach to reconstruct N-port S-matrix consists in evaluating an equivalent circuit from $N(N-1)/2$ S-matrix measurements at ports 1 and 2 of the N-port waveguide device. From the knowledge of the electrical parameters of the equivalent circuit, the S-matrix of the overall N-port device can be evaluated with simple manipulations.

The first step consists in drawing an equivalent circuit that is suitable to evaluate its electrical parameters from 2-port S-matrix measurements. The proposed circuit for a 4-port device is shown in Fig. 1(a), and it is derived from the equivalent circuits discussed in [22–25]. The transformers are used to normalize the admittances in the circuit kernel. The simple application of the equivalent circuits proposed in [25] is useless because it is quite hard to obtain the electrical parameters of those circuits from 2-port S-matrix measurements at ports 1 and 2. In fact, if we load ports 3 and 4 of the circuit discussed in [25] with $N(N-1)/2$ combinations of two loads, the evaluation of the electrical parameters is obtained solving ten nonlinear equations, containing ten scattering parameters of the 4-port S-matrix. Hence, that circuit is unable to solve this problem efficiently, and another equivalent circuit should be defined, recalling that many equivalent circuits can be defined for the same device, each of them satisfying a particular property (frequency dependence, simplicity, parameter reduction...) [20, 21].

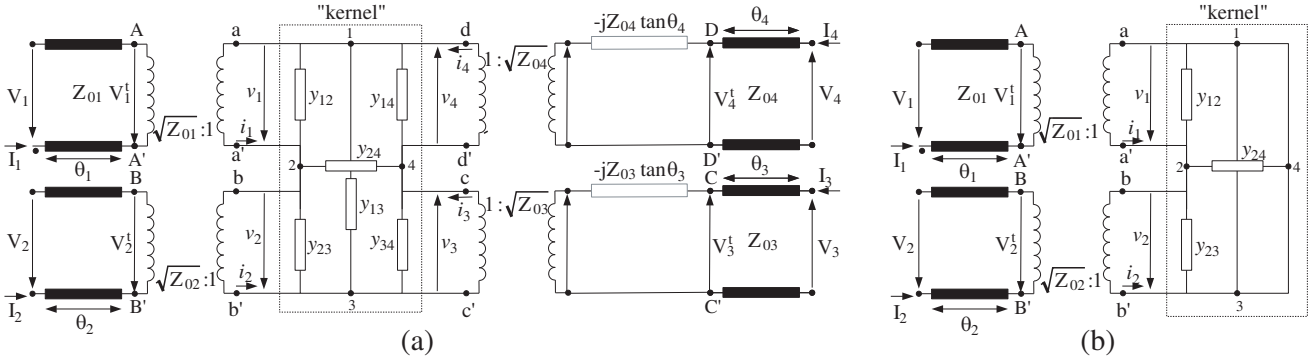

Figure 1. (a) The equivalent circuit of a 4-port device. (b) The reduced equivalent circuit of the 4-port device when two short circuits are connected to ports 3 and 4 of the circuit shown in Fig. 1(a).

Following this advice, the kernel of the circuit shown in Fig. 1(a) (i.e., the admittances placed at the sides and at the symmetry axes of the rectangle) and the two lines connecting the kernel to the measurement ports 1 and 2 are the same of [25], redrawn and rearranged for convenience. The difference is the presence of the series impedances $-jZ_{0k}\tan\theta_k$, $k = 3, 4$ between the kernel and connecting lines of the loaded ports 3 and 4. These series impedances are the key to simplify the evaluation of the circuit parameters (lines and admittances) from 2-port S-matrix measurements done at ports 1 and 2.

In fact, let's suppose to load ports 3 and 4 of the circuit shown in Fig. 1(a) with two shorts. The impedances seen at sections CC′ and DD′ are respectively $jZ_{03}\tan\theta_3$ and $jZ_{04}\tan\theta_4$, which resonate with the series impedances $-jZ_{0k}\tan\theta_k$, $k = 3, 4$, resulting in two short circuits at sections cc′ and dd′ of the kernel and a global short circuit between nodes 1 and 3. Hence, the equivalent circuits reduce to that shown in Fig. 1(b). If the same loads are connected to the actual device at ports 3 and 4, the corresponding 2-port S-matrix, $S^{0,0}$, can be measured at ports 1 and 2. The two superscript characters of S represent the two loads connected to ports 3 and 4. Hence, the electrical lengths θ_1, θ_2 and the

sum of the admittances connected to node 2

$$y_p = y_{12} + y_{23} + y_{24} \tag{11}$$

can be easily evaluated from this measurement, as described in [25] and here reported:

$$e^{j\theta_1} = \sqrt{-\frac{\sqrt{S_{22}^{0,0}}}{\sqrt{S_{11}^{0,0}}S_{12}^{0,0} + S_{11}^{0,0}\sqrt{S_{22}^{0,0}}}} \quad e^{j\theta_2} = \sqrt{\frac{S_{11}^{0,0}}{S_{22}^{0,0}}}e^{j\theta_1} \quad y_p = 2\frac{\sqrt{S_{11}^{0,0}S_{22}^{0,0}}}{S_{12}^{0,0}} \tag{12}$$

From the knowledge of θ_1 and θ_2, it is possible to evaluate the other electrical lengths θ_3 and θ_4. In fact, if port 4 of the circuit shown in Fig. 1(a) is connected to a short circuit, port 4 disappears, being short-circuited by the resonance of the input impedance and the series impedance $-jZ_{04}\tan\theta_4$. Moreover, if port 3 is connected to a *shorted* waveguide of length t_a, the circuit reduces to that shown in Fig. 2, with $k = (3)$. The normalized input admittance seen at section cc′ can be evaluated with simple mathematical manipulations, β being the propagation constant of the fundamental waveguide mode

$$y_{\text{input}}^{\text{sw}}(t_a, \theta_3) = j\frac{\sin(2\theta_3)}{2} - j\frac{\cos^2(\theta_3)}{\tan(\beta t_a)} \tag{13}$$

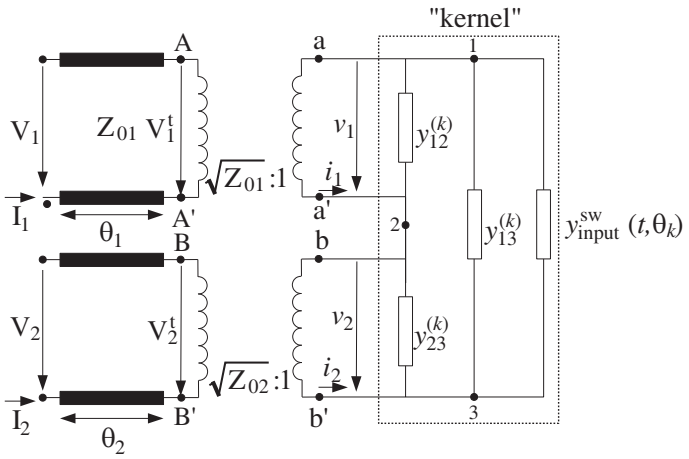

Figure 2. The equivalent circuit of the 4-port device shown in Fig. 1(a) with port 3 or 4 loaded with a short. If port 3 is connected to a load and port 4 is connected to a short, $k = (3)$ and the normalized admittances are: $y_{12}^{(3)} = y_{12} + y_{24}, y_{13}^{(3)} = y_{13} + y_{34}, y_{23}^{(3)} = y_{23}$. If port 4 is connected to a load and port 3 is connected to a short, $k = (4)$ and the normalized admittances are: $y_{12}^{(4)} = y_{12}, y_{23}^{(4)} = y_{23} + y_{24}, y_{13}^{(4)} = y_{13} + y_{14}$.

The admittance in Fig. 2 between nodes i and j, $y_{ij}^{(k)}$, when port k is loaded with a load and the other port with a short, is

$$y_{12}^{(3)} = y_{12} + y_{24} \qquad y_{13}^{(3)} = y_{13} + y_{34} \qquad y_{23}^{(3)} = y_{23} \tag{14}$$

The corresponding 2-port S-matrix, $S^{t_a,0}$, can be measured at ports 1 and 2, and the following manipulations can be done on the circuit shown in Fig. 2: (a) a line of electrical length $-\theta_1$ is added to port 1, to vanish the overall transmission line at the same port; (b) a line of electrical length $-\theta_2$ connected to a short circuit (*shorted* line) is added to port 2. The equivalent circuit is simplified as shown in Fig. 3(a). The normalized input admittance seen from section aa′, $y_{aa'}^{(3)}(t_a, 0)$, is:

$$y_{aa'}^{(3)}(t_a, 0) = \frac{i_1^{(3)}}{v_1^{(3)}} = y_{12}^{(3)} + y_{13}^{(3)} + y_{\text{input}}^{\text{sw}}(t_a, \theta_3) \tag{15}$$

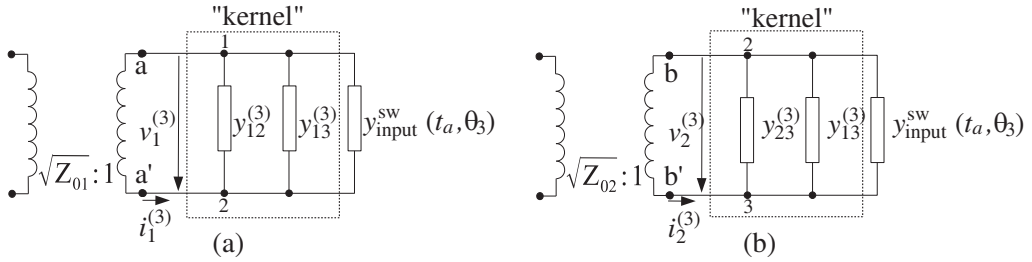

Figure 3. The equivalent circuit shown in Fig. 1(a) when port 4 is connected to a short circuit, port 3 to a *shorted* waveguide of length $t_{\rm a}$, and (a) port 2 to a *shorted* line of electrical length $-\theta_2$ and port 1 to a line of electrical length $-\theta_1$; or (b) port 2 to a line of electrical length $-\theta_2$ and port 1 to a *shorted* line of length $-\theta_1$.

Obviously, the same transformation can be mathematically applied to the measured 2-port S-matrix, $S^{t_{\rm a},0}$, obtaining the corresponding value of $y_{\rm aa'}^{(3)}(t_{\rm a},0)$:

$$y_{\rm aa'}^{(3)}(t_{\rm a},0) \;=\; y_{12}^{(3)} + y_{13}^{(3)} + y_{\rm input}^{\rm sw}(t_{\rm a},\theta_3) = \frac{1-\Gamma_{\rm aa'}^{t_a,0}}{1+\Gamma_{\rm aa'}^{t_a,0}} \tag{16}$$

$$\Gamma_{\rm aa'}^{t_a,0} \;=\; e^{2j\theta_1}\left[S_{11}^{t_{\rm a},0} - \frac{e^{2j\theta_2}\left(S_{12}^{t_{\rm a},0}\right)^2}{1+e^{2j\theta_2}S_{22}^{t_{\rm a},0}}\right] \tag{17}$$

Similarly, adding a *shorted* line of electrical length $-\theta_1$ to port 1 and a line of electrical length $-\theta_2$ to port 2, the equivalent circuit is simplified as shown in Fig. 3(b), and the normalized input admittance seen from section bb′, $y_{\rm bb'}^{(3)}(t_{\rm a},0)$, is:

$$y_{\rm bb'}^{(3)}(t_{\rm a},0) \;=\; \frac{i_2^{(3)}}{v_2^{(3)}} = y_{23}^{(3)} + y_{13}^{(3)} + y_{\rm input}^{\rm sw}(t_{\rm a},\theta_3) = \frac{1-\Gamma_{\rm bb'}^{t_{\rm a},0}}{1+\Gamma_{\rm bb'}^{t_{\rm a},0}} \tag{18}$$

$$\Gamma_{\rm bb'}^{t_{\rm a},0} \;=\; e^{2j\theta_2}\left[S_{22}^{t_{\rm a},0} - \frac{e^{2j\theta_1}\left(S_{12}^{t_{\rm a},0}\right)^2}{1+e^{2j\theta_1}S_{11}^{t_{\rm a},0}}\right] \tag{19}$$

Equations (16) or (18) are the key to find θ_3. In fact, if we load port 4 with a short circuit and port 3 with a second *shorted* waveguide of length $t_{\rm b}$ and measure the corresponding S-matrix, $S^{t_{\rm b},0}$, from Eqs. (16) and (18) we can write:

$$y_{\rm aa'}^{(3)}(t_{\rm b},0) \;=\; y_{12}^{(3)} + y_{13}^{(3)} + y_{\rm input}^{\rm sw}(t_{\rm b},\theta_3) = \frac{1-\Gamma_{\rm aa'}^{t_{\rm b},0}}{1+\Gamma_{\rm aa'}^{t_{\rm b},0}} \tag{20}$$

$$y_{\rm bb'}^{(3)}(t_{\rm b},0) \;=\; y_{23}^{(3)} + y_{13}^{(3)} + y_{\rm input}^{\rm sw}(t_{\rm b},\theta_3) = \frac{1-\Gamma_{\rm bb'}^{t_{\rm b},0}}{1+\Gamma_{\rm bb'}^{t_{\rm b},0}} \tag{21}$$

where $\Gamma_{\rm aa'}^{t_{\rm b},0}, \Gamma_{\rm bb'}^{t_{\rm b},0}$ are obtained from Eqs. (17) and (19), replacing $t_{\rm a}$ with $t_{\rm b}$ and $S^{t_{\rm a},0}$ with $S^{t_{\rm b},0}$. Hence, from Eqs. (13), (16), (20)

$$\theta_3 = \arccos\left[\pm\sqrt{\frac{y_{\rm aa'}^{(3)}(t_{\rm a},0) - y_{\rm aa'}^{(3)}(t_{\rm b},0)}{j\cot(\beta t_{\rm b}) - j\cot(\beta t_{\rm a})}}\right] = \arccos\left[\pm\sqrt{\frac{\dfrac{1-\Gamma_{\rm aa'}^{t_a,0}}{1+\Gamma_{\rm aa'}^{t_a,0}} - \dfrac{1-\Gamma_{\rm aa'}^{t_{\rm b},0}}{1+\Gamma_{\rm aa'}^{t_{\rm b},0}}}{j\cot(\beta t_{\rm b}) - j\cot(\beta t_{\rm a})}}\right] \tag{22}$$

If the *shorted* waveguide of length t_b is replaced by a matched waveguide, the normalized admittance seen at section cc′ is

$$y_{\mathrm{input}}^{\mathrm{mw}}(\theta_3) = \frac{1}{1 - j\tan(\theta_3)} \tag{23}$$

and $y_{\mathrm{input}}^{\mathrm{mw}}$ replaces $y_{\mathrm{input}}^{\mathrm{sw}}$ in Figs. 2 and 3. Moreover, Eq. (22) becomes

$$\theta_3 = \arccos\left[\pm\sqrt{\frac{\dfrac{1-\Gamma_{\mathrm{aa'}}^{t_a,0}}{1+\Gamma_{\mathrm{aa'}}^{t_a,0}} - \dfrac{1-\Gamma_{\mathrm{aa'}}^{\mathrm{mw},0}}{1+\Gamma_{\mathrm{aa'}}^{\mathrm{mw},0}}}{-1 - j\cot(\beta t_\mathrm{a})}}\right] \tag{24}$$

$$\Gamma_{\mathrm{aa'}}^{\mathrm{mw},0} = e^{2j\theta_1}\left[S_{11}^{\mathrm{mw},0} - \frac{e^{2j\theta_2}(S_{12}^{\mathrm{mw},0})^2}{1 + e^{2j\theta_2}S_{22}^{\mathrm{mw},0}}\right] \tag{25}$$

$S^{\mathrm{mw},0}$ being the 2-port S-matrix measured with ports 3 and 4 loaded with a matched waveguide and a short circuit, respectively.

Similarly, the value of the electrical length θ_4 can be obtained by loading port 3 with a short circuit that simplifies the equivalent circuit as shown in Fig. 2, with $k = (4)$. Loading port 4 with two *shorted* waveguides of lengths t_a and t_b, or a *shorted* waveguide of length t_a and a matched load, and defining $S^{0,t_\mathrm{a}}, S^{0,t_\mathrm{b}}, S^{0,\mathrm{mw}}$ the corresponding measured 2-port S-matrices, Equations (16)–(21) become

$$y_{\mathrm{aa'}}^{(4)}(0,t_\mathrm{a}) = y_{12}^{(4)} + y_{13}^{(4)} + y_{\mathrm{input}}^{\mathrm{sw}}(t_\mathrm{a},\theta_4) = \frac{1-\Gamma_{\mathrm{aa'}}^{0,t_\mathrm{a}}}{1+\Gamma_{\mathrm{aa'}}^{0,t_\mathrm{a}}} \tag{26}$$

$$y_{\mathrm{aa'}}^{(4)}(0,t_\mathrm{b}) = y_{12}^{(4)} + y_{13}^{(4)} + y_{\mathrm{input}}^{\mathrm{sw}}(t_\mathrm{b},\theta_4) = \frac{1-\Gamma_{\mathrm{aa'}}^{0,t_\mathrm{b}}}{1+\Gamma_{\mathrm{aa'}}^{0,t_\mathrm{b}}} \tag{27}$$

$$y_{\mathrm{bb'}}^{(4)}(0,t_\mathrm{a}) = y_{23}^{(4)} + y_{13}^{(4)} + y_{\mathrm{input}}^{\mathrm{sw}}(t_\mathrm{a},\theta_4) = \frac{1-\Gamma_{\mathrm{bb'}}^{0,t_\mathrm{a}}}{1+\Gamma_{\mathrm{bb'}}^{0,t_\mathrm{a}}} \tag{28}$$

$$y_{\mathrm{bb'}}^{(4)}(0,t_\mathrm{b}) = y_{23}^{(4)} + y_{13}^{(4)} + y_{\mathrm{input}}^{\mathrm{sw}}(t_\mathrm{b},\theta_4) = \frac{1-\Gamma_{\mathrm{bb'}}^{0,t_\mathrm{b}}}{1+\Gamma_{\mathrm{bb'}}^{0,t_\mathrm{b}}} \tag{29}$$

$$y_{12}^{(4)} = y_{12} \qquad y_{23}^{(4)} = y_{23} + y_{24} \qquad y_{13}^{(4)} = y_{13} + y_{14} \tag{30}$$

with $\Gamma_{\mathrm{aa'}}^{0,t_\mathrm{a}}, \Gamma_{\mathrm{aa'}}^{0,t_\mathrm{b}}, \Gamma_{\mathrm{bb'}}^{0,t_\mathrm{a}}, \Gamma_{\mathrm{bb'}}^{0,t_\mathrm{b}}$ obtained from Eqs. (17) and (19), inverting superscripts t_a and 0 and replacing t_a with t_b. θ_4 can be obtained from Eq. (22) or (24), replacing $\theta_3, S^{t_\mathrm{a},0}, S^{t_\mathrm{b},0}, S^{\mathrm{mw},0}$ with $\theta_4, S^{0,t_\mathrm{a}}, S^{0,t_\mathrm{b}}, S^{0,\mathrm{mw}}$.

The evaluation of the kernel normalized admittances is quite simple. In fact, the susceptances connected to node 2, y_{12}, y_{23}, y_{24}, can be obtained from Eqs. (11), (12), (14), (16)–(21) and (26)–(30):

$$y_{12} = \frac{y_p + y_{\mathrm{aa'}}^{(4)}(0,t_\mathrm{a}) - y_{\mathrm{bb'}}^{(4)}(0,t_\mathrm{a})}{2} = \frac{y_p + \dfrac{1-\Gamma_{\mathrm{aa'}}^{0,t_\mathrm{a}}}{1+\Gamma_{\mathrm{aa'}}^{0,t_\mathrm{a}}} - \dfrac{1-\Gamma_{\mathrm{bb'}}^{0,t_\mathrm{a}}}{1+\Gamma_{\mathrm{bb'}}^{0,t_\mathrm{a}}}}{2} \tag{31}$$

$$y_{23} = \frac{y_p - y_{\mathrm{aa'}}^{(3)}(t_\mathrm{a},0) + y_{\mathrm{bb'}}^{(3)}(t_\mathrm{a},0)}{2} = \frac{y_p - \dfrac{1-\Gamma_{\mathrm{aa'}}^{t_a,0}}{1+\Gamma_{\mathrm{aa'}}^{t_a,0}} + \dfrac{1-\Gamma_{\mathrm{bb'}}^{t_\mathrm{a},0}}{1+\Gamma_{\mathrm{bb'}}^{t_\mathrm{a},0}}}{2} \tag{32}$$

$$y_{24} = \frac{1}{2}\left(\frac{1-\Gamma_{\mathrm{aa'}}^{t_a,0}}{1+\Gamma_{\mathrm{aa'}}^{t_a,0}} - \frac{1-\Gamma_{\mathrm{bb'}}^{t_\mathrm{a},0}}{1+\Gamma_{\mathrm{bb'}}^{t_\mathrm{a},0}} - \frac{1-\Gamma_{\mathrm{aa'}}^{0,t_\mathrm{a}}}{1+\Gamma_{\mathrm{aa'}}^{0,t_\mathrm{a}}} + \frac{1-\Gamma_{\mathrm{bb'}}^{0,t_\mathrm{a}}}{1+\Gamma_{\mathrm{bb'}}^{0,t_\mathrm{a}}}\right) \tag{33}$$

The remaining three admittances y_{34}, y_{14}, y_{13} can be evaluated with a linear equation system. In fact, two independent equations can be obtained from Eqs. (11), (12), (14), (16), (18), (26), (28), (30):

$$y_{13} + y_{34} = \frac{1}{2}\left(\frac{1-\Gamma_{\mathrm{aa'}}^{t_a,0}}{1+\Gamma_{\mathrm{aa'}}^{t_a,0}} - \frac{1-\Gamma_{\mathrm{bb'}}^{t_\mathrm{a},0}}{1+\Gamma_{\mathrm{bb'}}^{t_\mathrm{a},0}} - y_p\right) - y_{\mathrm{input}}^{\mathrm{sw}}(t_\mathrm{a}, \theta_3) \tag{34}$$

$$y_{13} + y_{14} = \frac{1}{2}\left(\frac{1-\Gamma_{\mathrm{aa'}}^{0,t_a}}{1+\Gamma_{\mathrm{aa'}}^{0,t_a}} - \frac{1-\Gamma_{\mathrm{bb'}}^{0,t_\mathrm{a}}}{1+\Gamma_{\mathrm{bb'}}^{0,t_\mathrm{a}}} - y_p\right) - y_{\mathrm{input}}^{\mathrm{sw}}(t_\mathrm{a}, \theta_4) \tag{35}$$

The third equation can be obtained loading ports 3 and 4 with a load combination not yet used and not containing short, chosen between cases (f)–(j) of Table 3, and measuring the corresponding S-matrix, S^{cross}, at ports 1 and 2. A simple manipulation is done on S^{cross}: two lines of electrical length $-\theta_1$ and $-\theta_2$ are connected to ports 1 and 2, to evaluate the S-matrix of the circuit kernel without the input/output lines, S^{ker}, as shown in Fig. 4(a). The voltages and currents at sections aa′ and bb′ of the circuit shown in Fig. 4(a) can be evaluated from the knowledge of S^{ker}, for any value of the scattering amplitudes a_1, a_2, which can be chosen arbitrarily. For example, if ports 3 and 4 are loaded with two *shorted* waveguides with lengths t_a and t_b. We set $a_1 = 1, a_2 = 1$, and we can write:

$$v_1 = a_1 + b_1 = 1 + S_{11}^{\mathrm{ker}} + S_{12}^{\mathrm{ker}} \qquad i_1 = a_1 - b_1 = 1 - S_{11}^{\mathrm{ker}} - S_{12}^{\mathrm{ker}} \tag{36}$$

$$v_2 = a_2 + b_2 = 1 + S_{21}^{\mathrm{ker}} + S_{22}^{\mathrm{ker}} \qquad i_2 = a_2 - b_2 = 1 - S_{21}^{\mathrm{ker}} - S_{22}^{\mathrm{ker}} \tag{37}$$

$$i_{12} = -y_{12}v_1 \qquad i_{23} = -y_{23}v_2 \qquad v_{24} = \frac{i_{24}}{y_{24}} = \frac{i_{12} + i_1 - i_2 - i_{23}}{y_{24}} \tag{38}$$

$$v_{14} = v_{24} - v_1 \qquad v_{13} = -v_1 - v_2 \tag{39}$$

It should be noted that the normalization of the scattering amplitudes with respect to the modal impedances $\sqrt{Z_{01}}$ and $\sqrt{Z_{02}}$ disappears in Eqs. (36)–(37) because sections aa′ and bb′ are placed at the output section of the transformers with ratio $\sqrt{Z_{01}} : 1$ and $\sqrt{Z_{02}} : 1$ shown in Fig. 4(a).

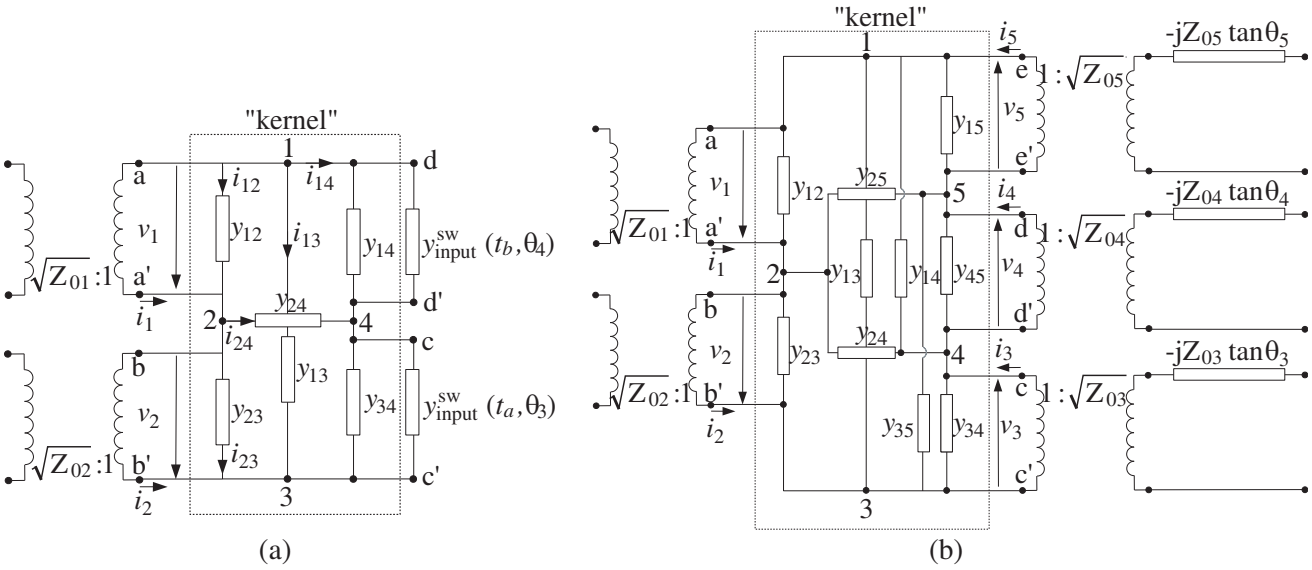

Figure 4. (a) The equivalent circuit of the 4-port device shown in Fig. 1(a) with ports 3 and 4 loaded with two different *shorted* waveguides of length t_a and t_b, port 2 with a line of length $-\theta_2$ and port 1 with a line of length $-\theta_1$. (b) The equivalent circuit of 5-port device. External lines have been omitted.

The equation at node 1 (or 3 or 4) is the third equation that must be written to find the last three unknown admittances y_{34}, y_{14}, y_{13}:

$$-i_1 = i_{13} + i_{12} + i_{14} = v_{13}y_{13} - v_1 y_{12} + v_{14}\left[y_{14} + y_{\mathrm{input}}^{\mathrm{sw}}(t_\mathrm{b}, \theta_4)\right] \tag{40}$$

v_{13}, v_1, v_{14} being known quantities, evaluated with Eqs. (36)–(39). Equations (40), (34) and (35) form a linear equation system in y_{34}, y_{14}, y_{13} that can be easily solved.

Summing up, the proposed approach permits to evaluate the electrical lengths θ_1, θ_2 connected to ports 1 and 2, loading ports 3 and 4 with two shorts, measuring the 2-port S-matrix $S^{0,0}$ and using Eq. (12). The other electrical lengths θ_3, θ_4 are obtained with Eq. (22) applied at port 3 (loading port 4 with a short and port 3 with two different *shorted* waveguides and measuring $S^{0,t_\mathrm{a}}, S^{0,t_\mathrm{b}}$) and at port 4 (loading port 3 with a short and port 4 with two different *shorted* waveguides and measuring $S^{t_\mathrm{a},0}, S^{t_\mathrm{b},0}$). The three admittances connected to node 2, shared by ports 1 and 2, are obtained with Eqs. (31)–(33). Finally, loading ports 3 and 4 with a load combination chosen between cases (f)–(j) in Table 3 and measuring S^{cross}, the remaining three admittances can be evaluated solving the linear equation system Eqs. (34), (35) and (40), with S^{ker} obtained from S^{cross}. The 4-port Z-matrix of the proposed equivalent circuit shown in Fig. 1(a) can be easily obtained and transformed in the 4-port S-matrix. The needed measurements are six.

In absence of experimental errors, the proposed approach gives the exact identification of the electrical parameters, while in presence of experimental errors some other steps are needed. In fact, any 2-port S-matrix suffers from measurement errors, and the number of error in the scattering parameters is unknown. Moreover, we can observe that when θ_1, θ_2 and the electrical length connected to port k are evaluated, we obtain three S-matrices (for example $S^{0,0}, S^{t_\mathrm{a},0}, S^{t_\mathrm{b},0}$ for $k = 3$) that are related by the property that only six scattering parameters are linearly independent, as discussed in Subsection 2.1. Hence, we can apply Eqs. (2)–(3) to evaluate the other three dependent scattering parameters. Obviously, which are the six most correct scattering parameters is unknown, hence a procedure similar to that described in Subsection 2.1 must be applied, taking into account all the combinations of the six independent scattering parameters and evaluating the corresponding electrical length θ_k and admittances $y^{\mathrm{k}}_{12}, y^{\mathrm{k}}_{23}, y^{\mathrm{k}}_{13}$ with Eqs. (14), (22), for each combination. The average of all combinations of each electrical parameter is applied to find the most correct value. This procedure must be applied to all N-2 ports.

The same approach can be extended to 5-port device, characterized by the equivalent circuit shown in Fig. 4(b), based on a 5-side polygon, with 10 admittances between nodes, similar to that discussed in [23] and here redrawn for convenience, with series impedances $-jZ_{0k}\tan\theta_\mathrm{k}$, $k = 3, 4, 5$ in the load ports. The external lines of length θ_k, $k = 1, \ldots, 5$ have been omitted. The procedure to evaluate the circuit parameters follows that previously discussed.

(i) Load ports 3, 4, 5 with 3 short loads and measure the S-matrix at ports 1 and 2, $S^{0,0,0}$, to obtain θ_1, θ_2 and y_p with Eq. (12), replacing $S^{0,0}_{ij}$ with $S^{0,0,0}_{ij}$, being $y_p = y_{12} + y_{23} + y_{24} + y_{25}$. (In this procedure, the superscript characters represent the sequence of loads connected to ports 3, 4, 5).

(ii) Load port 3 with two *shorted* waveguides of lengths t_a and t_b and ports 4, 5 with 2 short loads. Measure the two S-matrices, $S^{t_\mathrm{a},0,0}$ and $S^{t_\mathrm{b},0,0}$, evaluate $\Gamma^{t_\mathrm{a},0,0}_{\mathrm{aa}'}, \Gamma^{t_\mathrm{b},0,0}_{\mathrm{aa}'}$ with Eq. (17), replacing $S^{t_\mathrm{a},0}_{ij}$ with $S^{t_\mathrm{a},0,0}_{ij}$ or $S^{t_\mathrm{b},0,0}_{ij}$, to obtain θ_3 with Eq. (22), replacing $\Gamma^{t_\mathrm{a},0}_{\mathrm{aa}'}, \Gamma^{t_\mathrm{b},0}_{\mathrm{aa}'}$ with $\Gamma^{t_\mathrm{a},0,0}_{\mathrm{aa}'}, \Gamma^{t_\mathrm{b},0,0}_{\mathrm{aa}'}$.

(iii) Load port 4 with two *shorted* waveguides of lengths t_a and t_b and ports 3, 5 with 2 short loads. Measure the two S-matrices, $S^{0,t_\mathrm{a},0}$ and $S^{0,t_\mathrm{b},0}$, evaluate $\Gamma^{0,t_\mathrm{a},0}_{\mathrm{aa}'}, \Gamma^{0,t_\mathrm{b},0}_{\mathrm{aa}'}$ with Eq. (17), replacing $S^{t_\mathrm{a},0}_{ij}$ with $S^{0,t_\mathrm{a},0}_{ij}$ or $S^{0,t_\mathrm{b},0}_{ij}$, to obtain θ_4 with Eq. (22), replacing $\Gamma^{t_\mathrm{a},0}_{\mathrm{aa}'}, \Gamma^{t_\mathrm{b},0}_{\mathrm{aa}'}$ with $\Gamma^{0,t_\mathrm{a},0}_{\mathrm{aa}'}, \Gamma^{0,t_\mathrm{b},0}_{\mathrm{aa}'}$.

(iv) Load port 5 with two *shorted* waveguides of lengths t_a and t_b and ports 3, 4 with 2 short loads. Measure the two S-matrices, $S^{0,0,t_\mathrm{a}}$ and $S^{0,0,t_\mathrm{b}}$, evaluate $\Gamma^{0,0,t_\mathrm{a}}_{\mathrm{aa}'}, \Gamma^{0,0,t_\mathrm{b}}_{\mathrm{aa}'}$ with Eq. (17), replacing $S^{t_\mathrm{a},0}_{ij}$ with $S^{0,0,t_\mathrm{a}}_{ij}$ or $S^{0,0,t_\mathrm{b}}_{ij}$, to obtain θ_5 with Eq. (22), replacing $\Gamma^{t_\mathrm{a},0}_{\mathrm{aa}'}, \Gamma^{t_\mathrm{b},0}_{\mathrm{aa}'}$ with $\Gamma^{0,0,t_\mathrm{a}}_{\mathrm{aa}'}, \Gamma^{0,0,t_\mathrm{b}}_{\mathrm{aa}'}$.

(v) Evaluate the susceptances connected to node 2 of the circuit, with equations similar to Eqs. (31)–(33)

$$y_{12} = \frac{1}{2}\left(y_p + \frac{1-\Gamma^{0,0,t_\mathrm{a}}_{\mathrm{aa}'}}{1+\Gamma^{0,0,t_\mathrm{a}}_{\mathrm{aa}'}} - \frac{1-\Gamma^{0,0,t_\mathrm{a}}_{\mathrm{bb}'}}{1+\Gamma^{0,0,t_\mathrm{a}}_{\mathrm{bb}'}}\right) \qquad y_{23} = \frac{1}{2}\left(y_p - \frac{1-\Gamma^{t_\mathrm{a},0,0}_{\mathrm{aa}'}}{1+\Gamma^{t_\mathrm{a},0,0}_{\mathrm{aa}'}} + \frac{1-\Gamma^{t_\mathrm{a},0,0}_{\mathrm{bb}'}}{1+\Gamma^{t_\mathrm{a},0,0}_{\mathrm{bb}'}}\right) \quad (41)$$

$$y_{24} = \frac{1}{2}\left(\frac{1-\Gamma_{aa'}^{t_a,0,0}}{1+\Gamma_{aa'}^{t_a,0,0}} - \frac{1-\Gamma_{bb'}^{t_a,0,0}}{1+\Gamma_{bb'}^{t_a,0,0}} - \frac{1-\Gamma_{aa'}^{0,t_a,0}}{1+\Gamma_{aa'}^{0,t_a,0}} + \frac{1-\Gamma_{bb'}^{0,t_a,0}}{1+\Gamma_{bb'}^{0,t_a,0}}\right) \tag{42}$$

$$y_{25} = \frac{1}{2}\left(\frac{1-\Gamma_{aa'}^{0,t_a,0}}{1+\Gamma_{aa'}^{0,t_a,0}} - \frac{1-\Gamma_{bb'}^{0,t_a,0}}{1+\Gamma_{bb'}^{0,t_a,0}} - \frac{1-\Gamma_{aa'}^{0,0,t_a}}{1+\Gamma_{aa'}^{0,0,t_a}} + \frac{1-\Gamma_{bb'}^{0,0,t_a}}{1+\Gamma_{bb'}^{0,0,t_a}}\right) \tag{43}$$

(vi) Define 3 equations on the remaining six susceptances $y_{13}, y_{14}, y_{15}, y_{34}, y_{35}, y_{45}$, similar to (34), (35):

$$y_{34}+y_{35}+y_{13} = \frac{1}{2}\left(\frac{1-\Gamma_{aa'}^{t_a,0,0}}{1+\Gamma_{aa'}^{t_a,0,0}} - \frac{1-\Gamma_{bb'}^{t_a,0,0}}{1+\Gamma_{bb'}^{t_a,0,0}} - y_p\right) - y_{\text{input}}^{\text{sw}}(t_a,\theta_3) \tag{44}$$

$$y_{45}+y_{13}+y_{14} = \frac{1}{2}\left(\frac{1-\Gamma_{aa'}^{0,t_a,0}}{1+\Gamma_{aa'}^{0,t_a,0}} - \frac{1-\Gamma_{bb'}^{0,t_a,0}}{1+\Gamma_{bb'}^{0,t_a,0}} - y_p\right) - y_{\text{input}}^{\text{sw}}(t_a,\theta_4) \tag{45}$$

$$y_{13}+y_{14}+y_{15} = \frac{1}{2}\left(\frac{1-\Gamma_{aa'}^{0,0,t_a}}{1+\Gamma_{aa'}^{0,0,t_a}} - \frac{1-\Gamma_{bb'}^{0,0,t_a}}{1+\Gamma_{bb'}^{0,0,t_a}} - y_p\right) - y_{\text{input}}^{\text{sw}}(t_a,\theta_5) \tag{46}$$

(vii) Load ports 3, 4 with a combination of loads chosen between cases (f)–(j) of Table 3 and port 5 with a short load. Measure the S-matrix, $S^{t_a,t_b,0}$ for example, and add numerically two lines of length $-\theta_1$ and $-\theta_2$ to ports 1 and 2 to evaluate S^{ker}. The 5-port circuit is reduced to the 4-port circuit of Fig. 4(a) where node 5 becomes node 1, and the admittances between nodes 1 and 2, 1 and 3, 1 and 4 are $y_{12}+y_{25}$, $y_{13}+y_{35}$ and $y_{45}+y_{14}$, respectively. Write the linear equation corresponding to Eq. (40), with the help of Eqs. (36)–(39):

$$-i_1 = v_{13}(y_{13}+y_{35}) - v_1(y_{12}+y_{25}) + v_{14}\left[(y_{14}+y_{45}) + y_{\text{input}}^{\text{sw}}(t_b,\theta_4)\right] \tag{47}$$

(viii) Load ports 3, 5 with a combination of loads chosen between cases (f)–(j) of Table 3 and port 4 with a short load. Measure the S-matrix, $S^{t_a,0,t_b}$ for example, and add numerically two lines of length $-\theta_1$ and $-\theta_2$ to ports 1 and 2 to evaluate S^{ker}. The 5-port circuit is reduced to the 4-port circuit of Fig. 4(a) where node 5 becomes node 4, and the admittances between nodes 2 and 4, 3 and 4, 1 and 4 are $y_{24}+y_{25}$, $y_{34}+y_{35}$ and $y_{15}+y_{14}$, respectively. Write the linear equation corresponding to Eq. (40), with the help of Eqs. (36)–(39):

$$-i_1 = v_{13}y_{13} - v_1y_{12} + v_{14}\left[(y_{14}+y_{15}) + y_{\text{input}}^{\text{sw}}(t_b,\theta_5)\right] \tag{48}$$

(ix) Load ports 4, 5 with a combination of loads chosen between cases (f)–(j) of Table 3 and port 3 with a short load. Measure the S-matrix, S^{0,t_a,t_b} for example, and add numerically two lines of length $-\theta_1$ and $-\theta_2$ to ports 1 and 2 to evaluate S^{ker}. The 5-port circuit is reduced to the 4-port circuit of Fig. 4(a) where nodes 4 and 5 become nodes 3, and 4 and the admittances between nodes 2 and 3, 1 and 3, 3 and 4, 2 and 4 are $y_{24}+y_{23}$, $y_{14}+y_{13}$, $y_{35}+y_{45}$ and y_{25}, respectively. Write the linear equation corresponding to Eq. (40), with the help of Eqs. (36)–(39):

$$-i_1 = v_{13}(y_{13}+y_{14}) - v_1y_{12} + v_{14}\left[y_{14} + y_{\text{input}}^{\text{sw}}(t_b,\theta_5)\right] \tag{49}$$

(x) Equations (44)–(49) form a linear system on the remaining six susceptances.

The extension to N-port device is discussed in Appendix A.

3. RESULTS

3.1. Measurement Uncertainty

The two proposed methods could contain low reconstruction errors due to various problems, as the VNA intrinsic measurement uncertainty, uncertainty about the value of the matched load, actual lengths of the $\frac{\lambda}{8}$ (or $\frac{3\lambda}{8}$) shift waveguides and the connection between the flanges of the DUT and the loads connected to ports 3, 4, ..., N. These uncertainties could cause some errors in the reconstruction of the DUT S-matrix, and a discussion about their effects is fundamental to understand the limits of the proposed approaches. Hence, the 4-port WR-90 waveguide device shown in Fig. 5(b), a Tee magic with

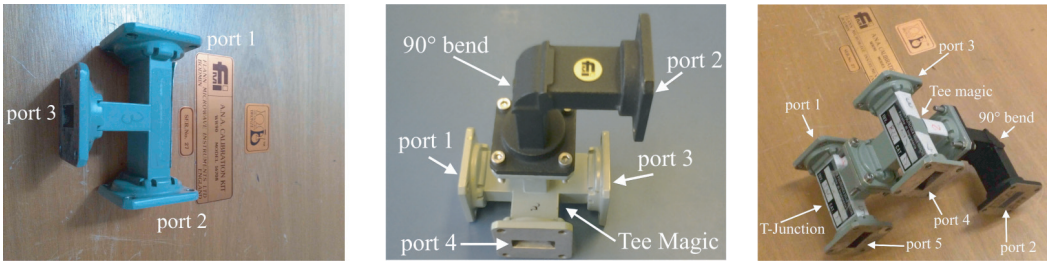

(a) (b) (c)

Figure 5. (a) E-plane T-junction; (b) Tee magic with 90° bend at port 2; (c) 5-port device obtained connecting a Tee magic and a T-junction. A 90° bend is connected to port 2 of (b) and (c) to avoid excessive bending of the coaxial cable connecting this port to VNA, through a coax-waveguide adapter.

90° bend at port 2, which will be analyzed in the next section, has been numerically simulated to obtain its 4-port S-matrix. Then, the 2-port VNA measurements have been numerically obtained connecting ports 3 and 4 of the numerical 4-port S-matrix to short, $\frac{\lambda}{8}$ (or $\frac{3\lambda}{8}$) shift waveguides, and matched loads, as discussed in the previous section. The possible measurement errors have been simulated as follows.

- To simulate the VNA intrinsic measurement uncertainty, the 2-port simulated measurements have been changed, adding a random error to the third, fourth or fifth decimal digit of each scattering parameter. Hence, $S_{ij}^{\text{measured}} = S_{ij}^{\text{exact}} + \delta_m 10^{-3} e^{j\delta_\phi}$, where S_{ij}^{exact} is the exact numerical scattering coefficient of the analyzed structure shown in Fig. 5(b), simulated with CST, and δ_m and δ_ϕ are random integers varying in the ranges $-9 \div 9$ and $0 \div 2\pi$, respectively. In doing so, a random error is added to the third decimal digit of each scattering parameter. To simulate the same error in the fourth or fifth decimal digit, 10^{-3} is replaced by 10^{-4} or 10^{-5}.
- To simulate the uncertainty of the value of the matched load, the corresponding 2-port simulated measurements have been obtained by loading port 3 or 4 with a numerical load with reflectivity equal to $-30\,\text{dB}$, $-40\,\text{dB}$ or $-50\,\text{dB}$, over the whole band of interest.
- To simulate the uncertainty due to the connections between the flanges of the loads and the DUT, the corresponding 2-port simulated measurements have been obtained by inserting a numerical load with reflectivity equal to $-40\,\text{dB}$ or $-50\,\text{dB}$ between the loads and the DUT.
- To simulate the uncertainty of the length of the $\frac{\lambda}{8}$, $\frac{3\lambda}{8}$ shift waveguides, an error equal to the mechanical precision has been taken into account. For example, if the mechanical precision is $\delta_l = 0.03\,\text{mm}$ (the same of our FLANN calibration kit), the corresponding 2-port simulated measurements have been obtained by loading port 3 or 4 with $\frac{\lambda}{8}$ or $\frac{3\lambda}{8}$ shift waveguides of actual lengths equal to $t_\text{a} = 4.835 \pm 0.03\,\text{mm}$ and $t_\text{b} = 14.458 \pm 0.03\,\text{mm}$, respectively.

Once the 2-port simulated measurements have been evaluated, they are used to reconstruct the 4-port S-matrix with the two approaches discussed in the previous section. The effects of the above uncertainties are analyzed in Fig. 6 where the difference between exact and reconstructed scattering coefficients with the S-direct approach, $\Delta S_{ij} = |S_{ij}^{\text{exact}} - S_{ij}^{\text{s}}|$, is shown for the case of the VNA uncertainty set at the third decimal digit. The main effect is recognizable on S_{24} (red curve of Fig. 6(b)) which should be less than $-80\,\text{dB}$ for the numerical Tee magic simulated with CST: the VNA uncertainty produces a maximum error of about 0.06 at 9.2 GHz on S_{24}, which is about $-24\,\text{dB}$ at this frequency. The other scattering coefficients, which are greater than zero, have an acceptable reconstruction error, as shown in the same figure. The reconstruction errors decrease if the VNA uncertainty is set to the fourth or the fifth decimal digit, as shown in the first three lines of Table 4, where: (a) $\Delta S_{24}^{\max}$ is the maximum difference between the reconstructed and the exact value of S_{24}; (b) $S_{24}^{\max}$ is the maximum value of the reconstructed value; (c) $\Delta S_{ij}^{\max}$ is the maximum difference between the reconstructed and the exact values of the other scattering coefficients, over the whole band. The best results are obtained with the VNA uncertainty set to the fifth decimal digit. For our Agilent 8510C network analyzer, the uncertainty can be assumed equal to the fourth decimal digit if the IF filter of the VNA is set to 1K, and this can be deduced comparing the values of measured S_{12} and S_{21} of a reciprocal device. In fact,

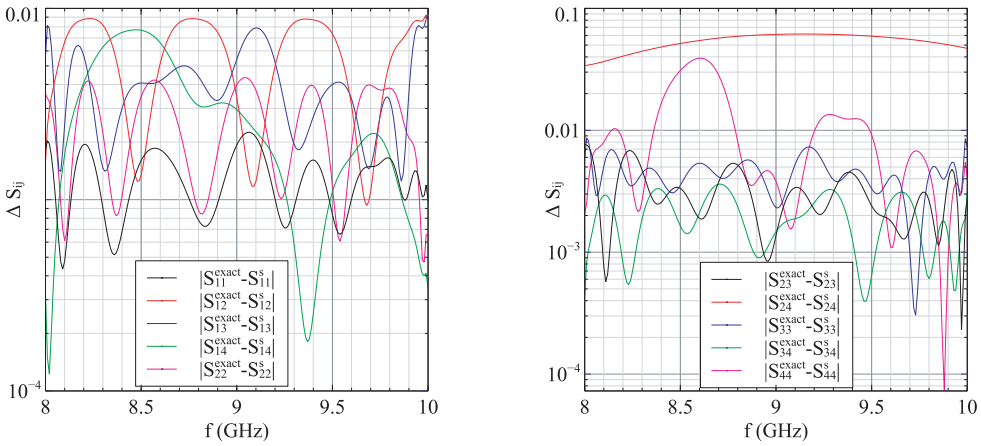

Figure 6. $\Delta S_{ij} = |S_{ij}^{exact} - S_{ij}^{s}|$ of the Tee magic shown in Fig. 5(b): S_{ij}^{exact} and S_{ij}^{s} are the scattering coefficients of the exact numerical 4-port S-matrix and of the reconstructed 4-port S-matrix with the S-direct approach, respectively. The curves refer to the VNA uncertainty at the third decimal digit.

Table 4. Analysis of measurement uncertainty for the structure shown in Fig. 5(b).

	ΔS_{24}^{max}		S_{24}^{max} (dB)		ΔS_{ij}^{max}	
Uncertainty	S approach	EC approach	S approach	EC approach	S approach	EC approach
VNA						
10^{-3}	0.062	0.014	−24.2	−36.8	0.038	0.014
10^{-4}	0.027	0.0012	−31.2	−58.4	0.015	0.0014
10^{-5}	0.009	0.0002	−41.2	−73.7	0.001	0.0002
Matched Load						
−30 dB	0.013	0.028	−37.5	−31.1	0.035	0.041
−40 dB	0.004	0.008	−47.6	−41.4	0.009	0.013
−50 dB	0.0012	0.003	−58	−51.7	0.003	0.004
Flange						
−40 dB	0.005	0.007	−47.6	−43.4	0.013	0.015
−50 dB	0.0013	0.004	−57.7	−53.7	0.004	0.005
$\frac{\lambda}{8}$ shifted waveguide length						
−0.03 mm	0.00006	0.0014	−140	−57.2	0.0046	0.0036
0.03 mm	0.00006	0.0014	−140	−57.2	0.0045	0.0036
$\frac{3\lambda}{8}$ shifted waveguide length						
−0.03 mm	0.00002	0.0020	−150	−54.3	0.0045	0.0026
0.03 mm	0.00002	0.0019	−150	−54.5	0.0046	0.0026

S_{12} and S_{21} differ in the third decimal digit if the IF filter is not set and in the fourth decimal digit if it is set to almost 1 K. Greater values of the IF filters produce a negligible improvement of the precision with a remarkable increase of the measurement time. Hence, with this choice, we can expect a value of the reconstructed S_{24} in the range $-30 \div -40$ dB.

The second uncertainty is due to the actual value of the matched load, as discussed above. The errors of the reconstructed value of the scattering parameters are reported in Table 4 in the lines relative to matched load, in the hypothesis of a matched load with values −30 dB, −40 dB or −50 dB over the whole band of interest: this uncertainty is less important than the previous one for the S-direct approach. Similar considerations apply to the uncertainty due to the connections between the flanges of the ports and the DUT (Table 4, lines relative to flanges).

Finally, the uncertainty on the mechanical precision (± 0.03 mm) of the length of the shifted waveguides is shown in Table 4 in the lines relative to $\frac{\lambda}{8}$ and $\frac{3\lambda}{8}$ shifted waveguide length. It is evident that this uncertainty can be considered irrelevant, for the S-direct approach.

The same simulations have been performed for the EC-approach, and the results are summarized in Table 4 in the columns relative to the EC-approach. For the EC-approach, the effect of the VNA uncertainty is less than the S-direct approach, while the effects of the matched load (if used, choosing cases (h)–(j) of Table 3) and of the flanges connection are greater than the S-direct approach. The effects of the lines' lengths are more pronounced than the S approach but always very low. From the previous discussion, we can consider to neglect the uncertainty due to the actual lengths of the shifted waveguide for both approaches, while the other uncertainties play different roles. In fact, the matched load and flanges uncertainties seem to afflict the S-matrix reconstruction more in the EC-approach than in the S-approach, while the opposite applies to the VNA uncertainty.

The analysis of the measurement uncertainty relative to the 5-port device shown in Fig. 5(c) is very similar and is not shown for brevity.

3.2. Experimental Results

The two proposed approaches have been applied to evaluate the S-matrices of 3-port, 4-port and 5-port WR-90 waveguide devices, shown in Fig. 5: an E-plane T-junction, a Tee magic and a Tee magic joined to a T-junction to obtain a 5-port device. A 90° bend is added to port 2 of Figs. 5(b) and 5(c), the second measurement port, to avoid an excessive bending of the coaxial cable connecting VNA to the coaxial-waveguide adapter. The loads in the FLANN calibration kit for WR-90 waveguide (Bronze series, serial number 27) have been used to load ports 3, 4 and 5. The *shorted* waveguides are obtained closing the $\frac{\lambda}{8}$ or the $\frac{3\lambda}{8}$ shift waveguide (lengths $t_a = 4.835$ mm and $t_b = 14.458$ mm, respectively) with a short (contained in the calibration kit).

The amplitude and phase of the reconstructed S_{ij} for the T-junction of Fig. 5(a) are shown in Fig. 7. For each amplitude of S_{ij}, two curves are shown in Fig. 7(a), the first (superscript s) referring to the S-direct approach and the second (superscript ec) to the EC-approach: the agreement is good. The agreement for the phases $\Phi_{ij} = \arg(S_{ij})$ of scattering coefficients is very good, as shown in Fig. 5(b), where the phase difference between the two approaches, $\Delta\Phi_{ij} = \Phi^s_{ij} - \Phi^{ec}_{ij}$, is reported.

The obtained results have been compared also with the experimental S-matrix of the T-junction, obtained closing one port at a time on a matched load and measuring the scattering coefficients occurring between the other two ports. Obviously, the experimental S-matrix suffers from some errors, as discussed

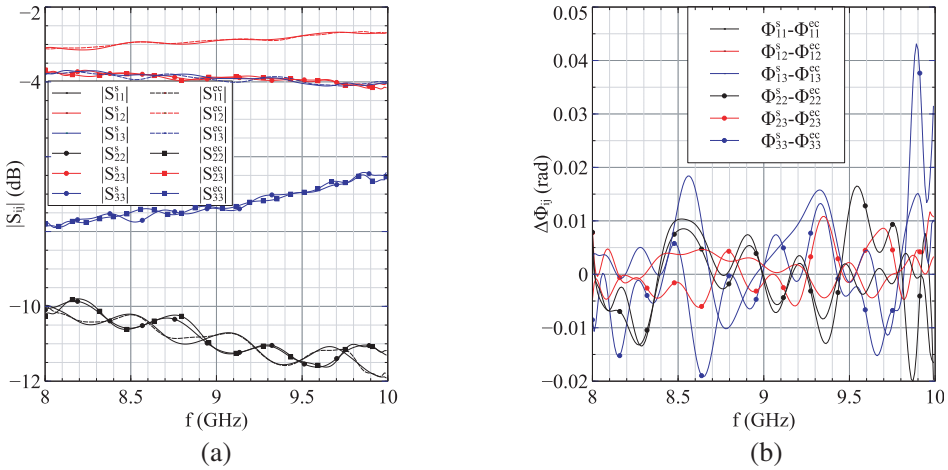

Figure 7. (a) Reconstruction of $|S_{ij}|$ of the E-plane T-junction, shown in Fig. 5(a). Two curves are shown for each scattering parameter, the first (superscript s) referring to the S-direct approach and the second (superscript ec) to the EC-approach. (b) Phase difference between the two approaches, $\Delta\Phi_{ij} = \Phi^s_{ij} - \Phi^{ec}_{ij}$.

Table 5. Comparison between reconstructed $|S_{ij}|$ and experimental values for the structures shown in Fig. 5 (worst case).

	Maximum deviation in whole band (dB)	Benchmark (experimental results)	Exceptions
E-plane T-junction, Fig. 5(a)			
$\lvert S_{ij}^{exp}\rvert_{dB} - \lvert S_{ij}^{s}\rvert_{dB}$	0.28	S_{33}	none
$\lvert S_{ij}^{exp}\rvert_{dB} - \lvert S_{ij}^{ec}\rvert_{dB}$	0.25	S_{33}	none
Tee-magic, Fig. 5(b)			
$\lvert S_{ij}^{exp}\rvert_{dB} - \lvert S_{ij}^{s}\rvert_{dB}$	0.34	S_{44}	S_{24}, see Fig. 8(b)
$\lvert S_{ij}^{exp}\rvert_{dB} - \lvert S_{ij}^{ec}\rvert_{dB}$	−0.32	S_{11}	S_{24}, see Fig. 8(b)
Tee-magic&T-junction, Fig. 5(c)			
$\lvert S_{ij}^{exp}\rvert_{dB} - \lvert S_{ij}^{s}\rvert_{dB}$	0.43	S_{45}	S_{12}, S_{25}, see Fig. 9(b)
$\lvert S_{ij}^{exp}\rvert_{dB} - \lvert S_{ij}^{ec}\rvert_{dB}$	−0.49	S_{11}	S_{12}, S_{25}, see Fig. 9(b)

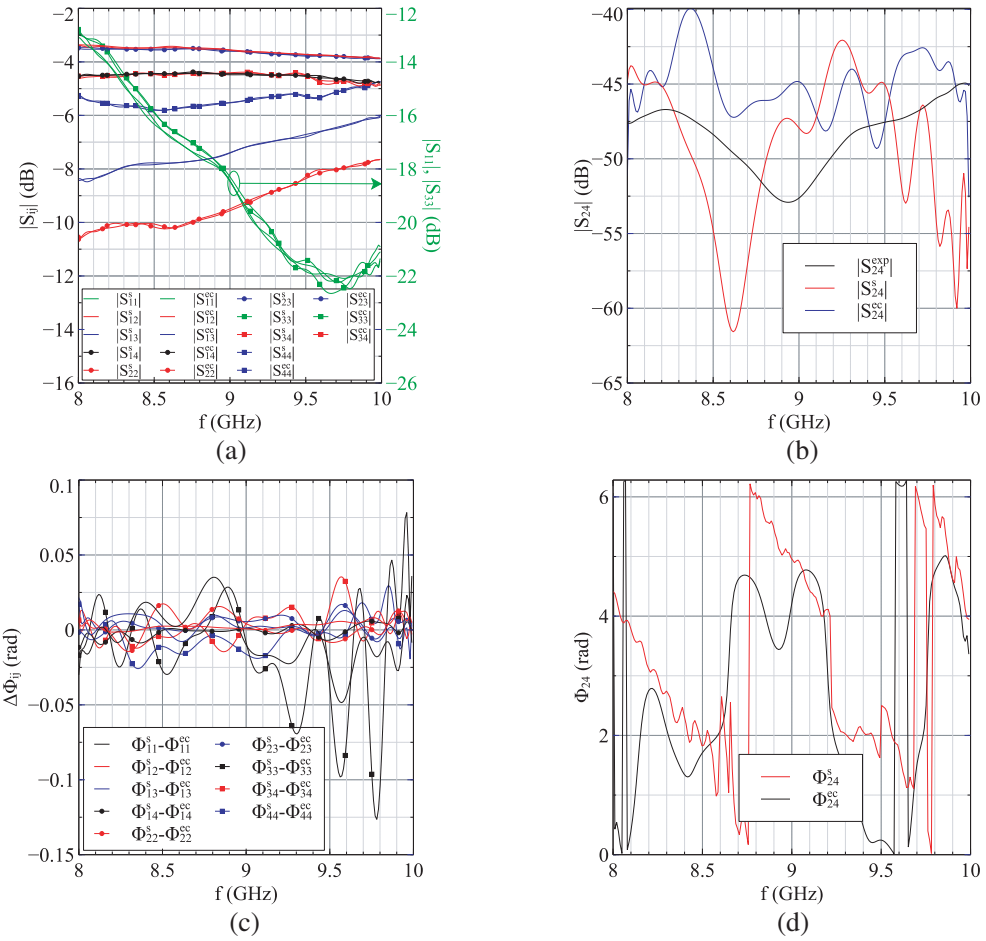

Figure 8. (a) and (b): reconstruction of $|S_{ij}|$ for the Tee magic with 90° bend at port 2, shown in Fig. 5(b). Two curves are shown for each scattering parameter, the first (superscript s) referring to the S-direct approach and the second (superscript ec) to the EC-approach. Experimental values of S_{24} are shown in (b). (c) Phase difference between the two approaches, $\Delta\Phi_{ij} = \Phi_{ij}^{s} - \Phi_{ij}^{ec}$, for all scattering parameters except S_{24}. (d) Φ_{24}^{s} and Φ_{24}^{ec}.

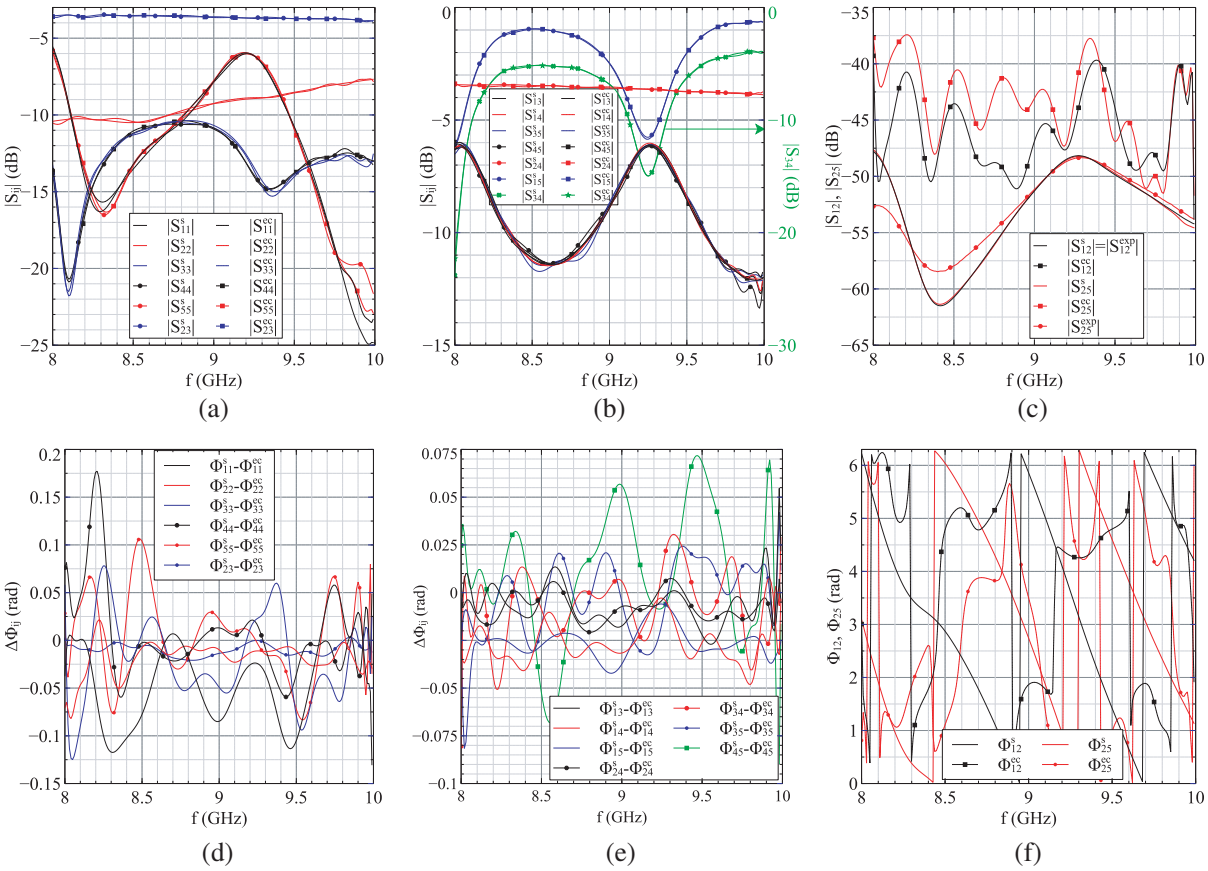

Figure 9. (a)–(c): reconstruction of $|S_{ij}|$ of the 5-port device, shown in Fig. 5(c). Two curves are shown for each scattering parameter, the first (superscript s) referring to the S-direct approach (Subsection 2.1) and the second (superscript ec) to the EC-approach (Subsection 2.2). Experimental values of S_{12} and S_{25} are shown in (c). (d)–(e): phase difference between the two approaches, $\Delta\Phi_{ij} = \Phi^s_{ij} - \Phi^{ec}_{ij}$, for all scattering parameters except for S_{12} and S_{25}. (f): $\Phi^s_{12}, \Phi^{ec}_{12}, \Phi^s_{25}$, and Φ^{ec}_{25}.

in the Introduction, due to the three disconnections and reconnections of the device. The reconstructed values of S_{ij} with the two proposed approaches have been compared with the experimental values, used as benchmark. This comparison is summarized in Table 5, where the worst case for all S_{ij} is reported: for the T-junction, the greater difference between the experimental (superscript exp) and reconstructed values, expressed in dB, $|S^{\exp}_{ij}|_{\mathrm{dB}} - |S^{s,ec}_{ij}|_{\mathrm{dB}}$, is less than 0.28 dB for $|S_{33}|$ in the worst case.

The amplitude and phase of the reconstructed S_{ij} for the 4-port Tee magic of Fig. 5(b) are shown in Fig. 8. The reconstructed values of $|S_{24}|$ are shown in Fig. 8(b), together with the experimental results, obtained with the same procedure used for the experimental results of the T-junction. The curves relative to $|S_{24}|$ are less than -40 dB, a very low value, and the reconstructed and experimental values show different behaviors. This effect is probably due to VNA, matched load and flanges uncertainties, which could interact with the reconstruction of very low values, as discussed in the previous subsection. The two approaches may give better results if precision dowels are used to connect the flanges of the FLANN coaxial-waveguide adapter (where dowels are present) and the flanges of the device under test (where dowels are not present). The values of $|S_{ij}|$ reconstructed with the two proposed approaches, except $|S_{24}|$ (col. 4), have been compared with the experimental values, used as benchmark, as shown in the rows of Table 5 relative to the Tee-magic: the greater difference between the reconstructed and experimental values is less than ± 0.35 dB for S_{44} (S-approach) or S_{11} (EC-approach) in the worst case.

For each phase of S_{ij}, except S_{24}, the difference between the phases reconstructed with the two approaches is shown in Fig. 8(c): the phase differences are very low, showing that the two proposed

approaches work quite well for the scattering coefficients with not negligible values. The reconstructed phase of S_{24} is shown in Fig. 8(d), and it is evident that there are different behaviors for the two approaches, due to the very low value of $|S_{24}|$.

The main problem in applying the S-direct approach to reconstruct N-port S-matrix is that this approach is expensive because of the cost of N-2 well calibrated and tested matched loads. On the contrary, the EC-approach could solve this problem, because N-2 shorts, not matched waveguides, are needed, and a low cost solution can be proposed, because a waveguide short can be simply realized in any mechanical laboratory starting from an aluminum substrate (or brass, bronze, ...) of some mm height. This was done in our laboratory, and one waveguide short was realized. Joining the waveguide calibration kit and this new waveguide short, the EC-approach can be applied to measure 5-port waveguide device. For the S-direct approach, a third calibrated matched waveguide must be used.

The results relative to the 5-port device of Fig. 5(c) are shown in Fig. 9: even in this case, the reconstruction of $|S_{ij}|$ with the two proposed approaches gives very similar results (Fig. 9(a)–9(b)). Small differences appear for $|S_{12}|$ and $|S_{25}|$ that have very low values, as shown in Fig. 9(c), where the experimental values are reported as benchmarks. It should be noted that the value of S_{12} is exact in the S-direct approach because it is directly measured when ports 3, 4 and 5 are connected to three matched loads. Hence, S_{12} obtained with the EC-approach contains reconstruction errors, due to its low value, and probably, the use of precision dowels at the 5 ports of the device could increase the precision of S_{12} reconstruction. It should be noted that with the S-direct approach, $|S_{12}| \approx |S_{25}|$, while with the EC approach these scattering coefficients show a similar behavior but with different values. The comparison of the reconstructed values of $|S_{ij}|$ with the experimental values, except for $|S_{12}|$ and $|S_{25}|$, is shown in the last two rows of Table 5, and the error is less than $\pm$ 0.5 dB, in the worst cases ($|S_{45}|$ and $|S_{11}|$), showing good agreement again.

4. CONCLUSIONS

Two different approaches (S-direct and Equivalent Circuit) have been proposed and discussed to reconstruct the S-matrix of N-port waveguide device, using a set of measurements performed always at the same 2-ports, loading the other N-2 ports with different loads. In doing so, the DUT must not be moved, reducing the number of movement cables. Moreover, hardware switching matrices, required in other approaches, are not used. The loads to be connected to the DUT are in a FLANN calibration kit for WR-90 waveguides and consist in two calibrated matched waveguides, two shorts and two calibrated different shifts ($\frac{\lambda}{8}$ and $\frac{3\lambda}{8}$ at center frequency of the X band). The first S-direct approach requires N-2 calibrated matched waveguides while the second EC-approach requires N-2 shorts, which can be easily realized in a mechanical laboratory, with very low cost and good precision. The results show very good agreement for both the approaches. Only the scattering parameters with very low value contain errors in their evaluation. These errors could be lowered if precision dowels are used to connect the flanges of the coaxial-waveguide adapter to the flanges of the device under test.

APPENDIX A.

The EC-approach can be extended to N-port device, characterized by $N(N+1)/2$ scattering parameters, defining an equivalent circuit based on a kernel obtained from a N-side polygon [25], with admittances between nodes, and connecting the sides relative to ports 1 and 2 to transmission lines of lengths θ_1 and θ_2 and the other N-2 sides to series impedances $-jZ_{0\mathrm{k}} \tan\theta_{\mathrm{k}}$ followed by transmission lines of length θ_{k}, $k = 3, 4, \ldots, N$. The procedure to evaluate the electrical parameters of the equivalent circuits is similar to that previously discussed: firstly, the electrical lengths $\theta_1, \theta_2, \ldots, \theta_N$ are evaluated, then the N-1 susceptances connected to node 2 are obtained, and finally, a linear system on the remaining admittances is solved. The steps are as follows:

(i) Load ports $3, 4, 5, \ldots, N$ with N-2 short loads and measure the S-matrix at ports 1 and 2 to obtain θ_1, θ_2 and y_p with Eq. (12), being $y_p = y_{12} + \sum_{i=3}^{N} y_{2i}$.

(ii) Load ports $3, 4, \ldots, N$ with N-3 short loads, except port k that is loaded with two *shorted* waveguides of lengths t_{a} and t_{b} or with a *shorted* waveguides of length t_{a} and a matched load.

Measure the corresponding two S-matrices at ports 1 and 2 to obtain $\theta_{\rm k}$ with Eq. (22) or (24) and repeat for $k = 3, 4, \ldots, N$. Moreover

$$y_{12} = \frac{y_p + y^{(\rm N)}_{\rm aa'}(t_{\rm a}) - y^{(\rm N)}_{\rm bb'}(t_{\rm a})}{2} \qquad y_{23} = \frac{y_p + y^{(3)}_{\rm bb'}(t_{\rm a}) - y^{(3)}_{\rm aa'}(t_{\rm a})}{2} \tag{A1}$$

$$y_{2i} = \frac{y^{(\rm i\text{-}1)}_{\rm aa'}(t_{\rm a}) - y^{(\rm i\text{-}1)}_{\rm bb'}(t_{\rm a}) - y^{(\rm i)}_{\rm aa'}(t_{\rm a}) + y^{(\rm i)}_{\rm bb'}(t_{\rm a})}{2} \tag{A2}$$

with $4 \le i \le N$. $y^{(\rm i)}_{\rm aa'}(t_{\rm a})$ and $y^{(\rm i)}_{\rm bb'}(t_{\rm a})$ are the admittances seen from section aa′ or bb′ when port i is connected to a *shorted* waveguides of length $t_{\rm a}$ and the other ports to a short (see Eqs. (16), (18) or (41)–(43)). In doing so, N electrical lengths and $N-1$ susceptances in Eqs. (A1)–(A2) can be evaluated. N-2 linear equations, corresponding to Eqs. (34)–(35) or (44)–(46), can also be written, with $3 \le i \le N$:

$$\sum_{m=3}^{i} \sum_{j=i+1}^{\rm N} y_{mj} + \sum_{j=3}^{i} y_{1j} = \frac{y^{(\rm i)}_{\rm aa'}(t_{\rm a}) - y^{(\rm i)}_{\rm bb'}(t_{\rm a}) - y_p}{2} - y^{\rm sw}_{\rm input}(t_{\rm a}, \theta_i) \tag{A3}$$

(iii) Load ports $3, 4, 5, \ldots, N$ with N-4 short loads, except ports i and j ($j > i$) that are loaded with two *shorted* waveguides of lengths $t_{\rm a}$ and $t_{\rm b}$ or with a *shorted* waveguides of length $t_{\rm a}$ and a matched load (cases (f)–(j) of Table 3). Measure the S-matrix $S^{i,j}_{\rm cross}$ at ports 1 and 2, evaluate the corresponding kernel matrix $S^{i,j}_{\rm ker}$ of the 2-port circuit, similar to that shown in Fig. 4(a), and write the corresponding Equation (40) at node 1:

$$\begin{aligned} -i_1 \;=\; & v_{13} \left(\sum_{m=3}^{i} y_{1m} + \sum_{m=3}^{i} \sum_{n=j+1}^{\rm N} y_{mn} \right) + v_{14} \left[\sum_{m=i+1}^{j} y_{1m} + \sum_{m=i+1}^{j} \sum_{n=j+1}^{\rm N} y_{mn} + y^{\rm sw}_{\rm input}(t_{\rm b}, \theta_j) \right] \\ & - v_1 \left(y_{12} + \sum_{m=j+1}^{\rm N} y_{2m} \right) \end{aligned} \tag{A4}$$

v_1, v_{13}, i_1 and v_{14} are voltages and currents similar to Eqs. (36)–(39), obtained with $S^{i,j}_{\rm ker}$. If a matched load is connected to port j, $y^{\rm mw}_{\rm input}(\theta_j)$ replaces $y^{\rm sw}_{\rm input}(t_{\rm b}, \theta_j)$ in Eq. (A4).
Repeat for $3 \le i \le N$ and $i+1 \le j \le N$.

The N-2 equation (A3) and $(N^2 - 5N + 6)/2$ equation (A4) form a linear system in the remaining admittances that can be easily solved. Once the $N(N+1)/2$ electrical parameters of the equivalent circuit have been evaluated, the Z-matrix of the circuit kernel can be obtained with KVL. The kernel S-matrix is obtained with $S = (\zeta + I)^{-1}(\zeta - I)$, ζ being the normalized Z-matrix, and the overall S-matrix is derived shifting the ports of the kernel S-matrix for an amount equal to $\theta_{\rm k}$ for $k = 1, 2, \ldots, N$.

REFERENCES

1. Franzen, N. R. and R. A. Speciale, "A new procedure for system calibration and error removal in automated s-parameter measurements," *5th European Microwave Conference*, 69–73, 1975.
2. Speciale, R. A. and C. Tzuang, "Test results on the new TSZ calibration method," *21st ARFTG Conference*, Vol. 3, 39–46, Jun. 1983.
3. Rolfes, I. and B. Schiek, "LRR-A self-calibration technique for the calibration of vector network analyzers," *IEEE Transactions on Instrumentation and Measurement*, Vol. 52, No. 2, 316–319, Apr. 2003.
4. Lenk, F., R. Doerner, and A. Rumiantsev, "Sensitivity analysis of s-parameter measurements due to calibration standards uncertainty," *IEEE Transactions on Microwave Theory and Techniques*, Vol. 61, No. 10, 3800–3807, Oct. 2013.
5. Stumper, U. and T. Schrader,, "Calibration method for vector network analyzers using one or two known reflection standards," *IEEE Transactions on Instrumentation and Measurement*, Vol. 63, No. 6, 1648–1655, Jun. 2014.

6. Morini, A., M. Guglielmi, and M. Farina, "A technique for the measurement of the generalized scattering matrix of overmoded waveguide devices," *IEEE Transactions on Microwave Theory and Techniques*, Vol. 61, No. 7, 2705–2714, Jul. 2013.
7. Tippet, J. and R. A. Speciale, "A rigorous technique for measuring the scattering matrix of a multiport device with a 2-port network analyzer," *IEEE Transactions on Microwave Theory and Techniques*, Vol. 30, No. 5, 661–666, May 1982.
8. Helton, J. and R. Speciale, "A complete and unambiguous solution to the super-TSD multiport-calibration problem," *IEEE MTT-S International Microwave Symposium*, 251–252, May 1983.
9. Rautio, J. C., "Techniques for correcting scattering parameter data of an imperfectly terminated multiport when measured with a two-port network analyzer," *IEEE Transactions on Microwave Theory and Techniques*, Vol. 31, No. 5, 407–412, May 1983.
10. Schoon, M., "A semi-automatic 3-port network analyzer," *IEEE Transactions on Microwave Theory and Techniques*, Vol. 41, No. 6, 974–978, Jun. 1993.
11. Davidovitz, M., "Reconstruction of the S-matrix for a 3-port using measurements at only two ports," *IEEE Microwave and Guided Wave Letters*, Vol. 5, No. 10, 349–350, Oct. 1995.
12. Sercu, S. and L. Martens, "Characterizing n-port packages and interconnections with a 2-port network analyzer," *IEEE 6th Topical Meeting on Electrical Performance of Electronic Packaging*, 163–166, Oct. 1997.
13. Lu, H.-C. and T.-H. Chu, "Multiport scattering matrix measurement using a reduced-port network analyzer," *IEEE Transactions on Microwave Theory and Techniques*, Vol. 51, No. 5, 1525–1533, May 2003.
14. Rolfes, I. and B. Schiek, "An efficient method for the measurement of the scattering-parameters of multi-ports with a two-port network-analyzer," *34th European Microwave Conference*, Vol. 2, 797–800, Oct. 2004.
15. Rolfes, I. and B. Schiek, "Multiport method for the measurement of the scattering parameters of n-ports," *IEEE Transactions on Microwave Theory and Techniques*, Vol. 53, No. 6, 1990–1996, Jun. 2005.
16. Heuermann, H., "Multiport s-parameter calculation from two-port network analyzer measurements with or without switch matrix," *67th ARFTG Conference*, 219–222, Jun. 2006.
17. Will, B., I. Rolfes, and B. Schiek, "Fully automated measurements of calibrated scattering parameters of multi-ports with a two-port network analyzer," *European Microwave Conference*, 242–245, Oct. 2007.
18. Chen, C.-J. and T.-H. Chu, "Accuracy criterion for S-matrix reconstruction transforms on multiport networks," *IEEE Transactions on Microwave Theory and Techniques*, Vol. 59, No. 9, 2331–2339, Sept. 2011.
19. Rautio, J. and M. Davidovitz, "Comments on "reconstruction of the s-matrix for a 3-port using measurements at only two ports" [and reply]," *IEEE Microwave and Guided Wave Letters*, Vol. 6, No. 4, 183, Apr. 1996.
20. Marcuvitz, N., *Waveguide Handbook*, Mc-Graw-Hill, New York, 1951.
21. Montgomery, C. G., R. H. Dicke, and E. M. Purcell, *Principles of Microwave Circuits*, McGraw-Hill, 1948.
22. Zappelli, L., "An equivalent circuit for discontinuities exciting evanescent accessible modes," *IEEE Transactions on Microwave Theory and Techniques*, Vol. 60, No. 5, 1197 –1209, May 2012.
23. Zappelli, L., "Circuit approach to the analysis of microwave discontinuities," *Progress In Electromagnetics Research B*, Vol. 53, 373–397, 2013.
24. Zappelli, L., "An equivalent circuit for thick centered irises in rectangular waveguide," *Proceedings of Numerical Electromagnetic Modelling and Optimization (NEMO)*, Pavia, 2014.
25. Zappelli, L., "Simple, fast, and effective identification of an equivalent circuit of a waveguide junction with n ports," *IEEE Transactions on Microwave Theory and Techniques*, Vol. 63, No. 1, 48–55, Jan. 2015.